Determination of Constitutive Relations of Fault Slip Based on Seismic Wave Analysis

地震波解析に基づく断層すべりの構成関係の決定

井 出 哲

学位論文

Determination of Constitutive Relations of Fault Slip

Based on Seismic Wave Analysis

地震波解析に基づく断層すべりの構成関係の決定

平成8年12月博士（理学）申請

東京大学大学院理学系研究科

地球惑星物理学専攻

井出　哲

Determination of Constitutive Relations of Fault Slip

Based on Seismic Wave Analysis

Submitted in Partial Fulfilment

of the Requirements for the Degree of

Doctor of Science

Satoshi Ide

December, 1996

Contents

Abstract

Constitutive relation is the boundary condition on fault plane and governs many aspects of earthquake failure, *i.e.* generation, propagation, and termination, as well as whole seismic cycles. Although several constitutive laws have been formulated based on laboratory rock experiments and applied to theoretical studies in various fields, no actual relation during natural earthquake is clarified. The 1995 Kobe earthquake is suitable for detailed kinematic analysis because many near-field strong motion records are available, and this enables the first evaluation of constitutive relations of natural earthquake. In this study, we determine spatio-temporal slip distribution on an assumed fault plane of the 1995 Kobe earthquake by waveform inversion, and then, solve elasto-dynamic equations using a finite difference method to determine stress distribution and constitutive relation on the fault plane. An inversion method based on Bayes Theorem is employed to obtain a spatio-temporal slip distribution, and is enable to ensure the objective uniqueness of the solution with numerous parameters and smoothing constraints. The slip distribution shows similarities with previously presented source models of this earthquake, one of which is the shallow large slip having long duration. This slip distribution is then used as part of the boundary condition in the finite difference calculation. The obtained time histories of slip and shear stress provide a constitutive relation at each point on the fault plane. They show slip-weakening relations almost everywhere on the fault plane, while slip-rate dependency is not clear. The slip-weakening behavior has a clear depth dependency indicating that the slip-weakening rate ($d\tau/du$) is smaller in the shallow crust than that in the deep crust, from the other view point this suggests that the critical slip-weakening displacement in the shallow crust is larger than that in the deep crust. This may be associated with the paucity of shallow seismicity observed in the source region of this earthquake as reported for many mature fault systems, and may be a common feature for shallow crustal earthquakes.

Chapter 1

Introduction

Detailed analyses of seismic sources has revealed their complexity, being unlikely to be represented as propagating uniform line dislocations at fixed velocities on rectangle fault planes. It is now widely accepted that an earthquake is composed of many small-scale subevents, or asperities and barriers, and the propagation of rupture is not uniform and can be highly irregular. A dynamic rupture process may be preceded by a slow nucleation process which can trigger foreshock seismicity, and after the termination of the dynamic rupture process, aftershocks and afterslip occur within source region and its neighborhood.

Earthquake sources also have large diversity; one earthquake may look like different from another even if both have similar magnitude values. Fig. 1-1 shows an obvious example of such diversity in the rupture histories of earthquakes of the same moment magnitude (M_w = 7.6) determined by the multiple deconvolution methods of Kikuchi and Kanamori [1991] using teleseismic waves. The rupture of the 1992 Nicaraguan earthquake continued about 100 s [Ide *et al.*, 1993], while the 1993 Kushiro-oki earthquake occurred within 10 s [Takeo *et al.*, 1993]. Their source time (moment rate) functions are quite different from each other; moreover different from that of a 'standard' earthquake of M_w = 7.6 [Utsu, 1984]. The Nicaraguan earthquake is a shallow interplate earthquake and categorized as a 'tsunami earthquake' [Kanamori, 1972] that produces anomalous larger tsunamis than expected from its surface magnitude M_s. On the other hand, the Kushiro-oki earthquake is a high stress drop earthquake in the subducting oceanic plate at a depth of 100 km. Is it possible to interpret such difference of their dynamic behavior on a united physical basis?

1

One useful way to interpret earthquake dynamics with its high complexity and diversity is the simplification of seismic source as illustrated in Fig. 1-2.   Generally, an earthquake occurs on several fault planes within a plate, and/or on a plate interface.   These planes have many kinks or jogs and form a fault zone having a certain thickness, which are successfully approximated as a fault plane with no thickness if we analyze with seismic waves of larger wavelength than the fault zone thickness. An elastic material is also a good approximation of the surrounding body as long as the dynamic rupture processes of earthquakes are considered.   Thus, an earthquake source is represented by an elastic body and its boundary on which constitutive relations controlling earthquake complexity and diversity are given as boundary conditions.   Elastic properties in the surrounding body also control the source behavior, but their effects may be limited compared to the flexibility of constitutive relation. Using this simplification, any complexity or diversity of earthquake dynamics should be attributed to those in the constitutive relation on the fault plane.

Up until now, many studies presented various constitutive relations theoretically or based on laboratory experiments of rock friction in which frictional sliding is regarded as an analog to fault slip in natural earthquakes.   The most simple constitutive relation is the classical friction law having only static and dynamic friction levels, which results in the singularity of stress at the crack tip when it is introduced as a boundary condition of the crack surface.   To mathematically eliminate this singularity, the slip-weakening friction was introduced by Ida [1972] using the notion of a crack tip cohesive zone introduced by Barenblatt [1959] for tensile cracks.   As shown in Fig. 1-3a, this relation is characterized by four parameters: an initial stress τ_0, a peak stress τ_p, a residual, or dynamic, stress τ_r, and a critical displacement D_c.   Andrews [1976, 1985] applied this relation into the calculation of 2-D anti-plane shear crack propagation, while Day [1982] applied it into 3-D calculation.   From the experimental observation of temporal change of shear stress and frictional sliding amount during stick-slip instability along a precut fault in rock sample, Okubo and Dieterich

2

[1984] and Ohnaka *et al*. [1987] (Fig. 1-3b) proved the existence of the slip-weakening relations. Further, Matsu'ura *et al*. [1992] interpreted these relations by considering the microscopic interaction between statistically self-similar fault surfaces and presented a slip-dependent constitutive relation. Using such a slip-dependent constitutive relation, Shibazaki and Matsu'ura [1992, 1995] simulated the nucleation process of earthquakes.

Another frequently applied constitutive relation is the rate- and state-dependent friction law first presented by Dieterich [1979] and mathematically refined by Ruina [1983].   The advantage of this law over the slip-dependent constitutive relation is that the rate- and state-dependent law allows the retrieval of fault strength following a dynamic rupture because this contains velocity-weakening stress relation.   Therefore, it is applied in numerical simulations of long-term duration, *e.g.*, the seismic cycle [Tse and Rice, 1986; Rice, 1993] and the afterslip [Marone *et al.*, 1991].   Although this relation behaves differently from the slip-weakening relation when it is applied to the phenomena of long duration or those having velocity as low as the seismic nucleation process [Dieterich, 1992], Okubo [1989] showed that it produces a quite similar dynamic crack propagation to those with a slip-weakening relation.   Since the present study deals with dynamic rupture of earthquake, I assume the constitutive relations as the relations between fault slip and shear stress, namely as a slip-dependent relation.   Other than experimentally based constitutive relations, the slip-rate-dependent friction law is applied in the statistical study of seismicity [Carlson and Langer, 1989] and dynamic rupture propagation [Cochard and Madariaga, 1994; Beeler and Tullis, 1996] to explain a slip-pulse-like propagation of fault rupture.   To verify the possibility of slip-rate-dependent relations, the relations between the slip-rate and shear stress are discussed.

In spite of its significance in the many theoretical studies referred to above, the constitutive relation has not been estimated for the faulting process of natural earthquakes.   The scaling relation between experimentally derived constitutive relations and those of natural earthquake is also

3

unknown.   An exception is the study about critical displacement D_c of slip-weakening (Fig. 1-3a), based on the specific barrier model of Papageorgiou and Aki [1984].   Since D_c is a parameter that determines the stress concentration near crack tip and the radiation of high frequency waves, they estimated D_c in the range from 0.4 to 4 m using the estimation of cutoff of acceleration spectra at high frequency.   In the present paper, I try to obtain not only D_c but also the shape of constitutive relations between slip and shear stress on a fault plane, namely as a slip-dependent relation.

Previous studies of the earthquake source process have been mainly kinematic ones, in which the spatio-temporal distribution of slip is determined on assumed fault planes.   To determine the constitutive relations, the spatio-temporal distribution of stress is also necessary.   The dynamic models presented by Quin [1990] and Miyatake [1992] determined the stress distribution during earthquake rupture based on the linear elasticity theory with crack propagation and classical friction law of static and dynamic friction levels.   In these dynamic models, the kinematic parameters, slip amount and rupture time, are converted to dynamic parameters, static and dynamic stress level on the fault plane.   Although these approaches has been the only way to estimate the stress-field on the fault plane, there are some defects, $i.e.$, 1) stress and slip-rate singularity at the crack tip due to the assumption of classical friction law, 2) non-uniqueness arising from subjectivity due to the insufficient information from kinematic model, and 3) the difficulty in explaining detailed kinematic models because a part of the procedure is resolved by try-and-error method.   In addition, the third defect result in the difficulty to construct such a dynamic model that can explain the observed seismic waves, though Fukuyama and Mikumo [1993] and Ide and Takeo [1996] proposed iterative modeling methods for this purpose.   The approach to obtain the stress-field in the present study is different from the above dynamic modeling method and can overcome all the above three defects.   I determine stress distribution directly from a kinematic model, in which stress and slip-rate are always finite, the result is based on an objectively unique kinematic model which is more detailed than the

4

kinematic model used in the previous dynamic modeling.

The procedure is divided into two successive calculations. First, we invert seismic waves to obtain the spatio-temporal slip distribution and then solve the elasto-dynamic equations to obtain the spatio-temporal stress distribution. Fig. 1-4 illustrates the comparison between the laboratory experiment and my method to obtain constitutive relations. In the laboratory experiments of stick-slip instability [Okubo and Dieterich, 1984; Ohnaka *et al.*, 1987], slip and shear stress are individually measured by strain meters located along a precut fault in the rock sample. By monitoring these meters during stick-slip instability, a local slip-stress relation is obtained at each point on the fault plane. On the other hand, in the analysis of natural earthquake the only quantity obtained by waveform inversion is the distribution of slip. Nevertheless, the stress distribution can be obtained by solving elasto-dynamic equations with the boundary conditions of slip distribution. I employ finite difference method (FDM) for the calculation of the elasto-dynamic equations. By comparing them at each time step, a local slip-stress relation is determined at each point on the fault plane.

The target earthquake is the 1995 Kobe (Hyogo-ken Nanbu), Japan, earthquake (Ms 6.8); a shallow intra-plate strike-slip earthquake which was recorded at numerous near-field stations. The hypocentral depth determined by Japan Meteorological Agency (JMA) is 14 km. Fig. 1-5 shows the hypocentral location determined by JMA together with the aftershock distribution [Hirata *et al.*, 1996], the automated CMT solution determined by Earthquake Research Institute [Kawakatsu, 1995], and the active fault traces [The Research Group for Active Faults in Japan, 1991]. Until now, some kinematic models have been presented [Ide *et al.*, 1996a; Horikawa *et al*, 1996; Sekiguchi *et al.*, 1996; Wald, 1996; Yoshida *et al*, 1996], which are summarized in Table 1-1. Although the models are determined on different conditions with different data set, all the seismic moments are estimated as almost 2.0×10^{19} Nm. The spatial patterns of slip are similar in the point that the large slipped area is shallow southwest region southwest of the hypocenter and the region near the hypocenter.

In the northeast of the hypocenter all models show relatively smaller slip at deeper part of the fault plane than in the southwest of the hypocenter.

A clear dependency exists between the amount the maximum slip and the assumed fault area, *i.e.*, small faults result large maximum slips [Ide *et al.*, 1996a; Horikawa *et al.*, 1996; Yoshida *et al.*, 1996], whereas large faults produces small maximum slips [Sekiguchi *et al.*, 1996; Wald, 1996]. This may be mostly due to the smoothing constraints introduced into each study, suggesting the importance to judge the appropriateness of the smoothing weights.   Since the smoothness of the slip distribution is significant in calculation of stress field, I take care for this in the inversion analysis by application of the Bayesian modeling.
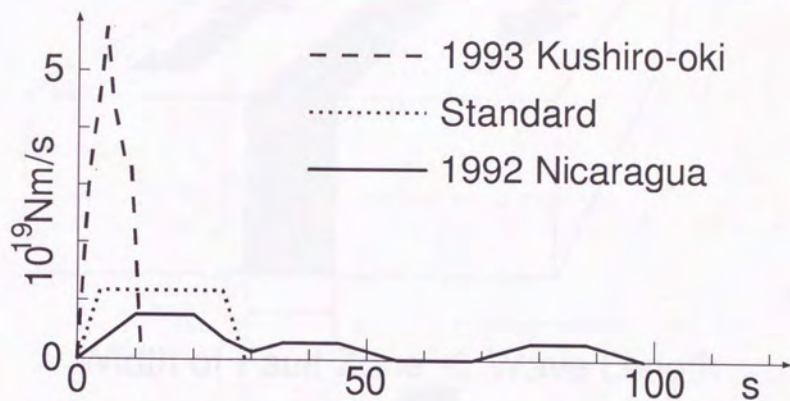
Fig. 1-1. Comparison of source time (moment rate) functions of three earthquake of the same moment

magnitude, *i.e.*, the 1992 Nicaraguan earthquake [Ide *et al.*, 1993], the 1993 Kushiro-oki earthquake

[Takeo *et al.*, 1993], and a 'standard' earthquake calculated the scaling relation of Utsu [1984].

Seismic Source

Width of Fault Zone $<$ Wave Length

Fault Zone＝Fault Plane

Slip

Elastic Body

Traction

Constitutive Relation＝Boundary Condition
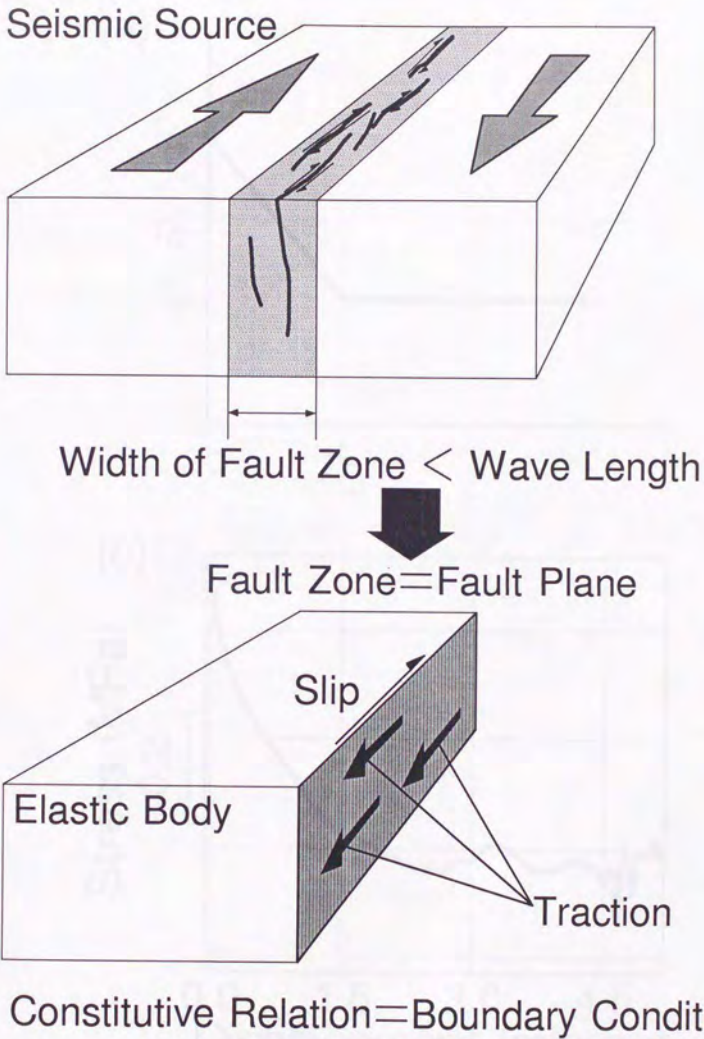
Fig. 1-2. Schematic representation of the assumption of seismic source as an elastic body and a fault plane with no thickness.

8

(a)

(b)
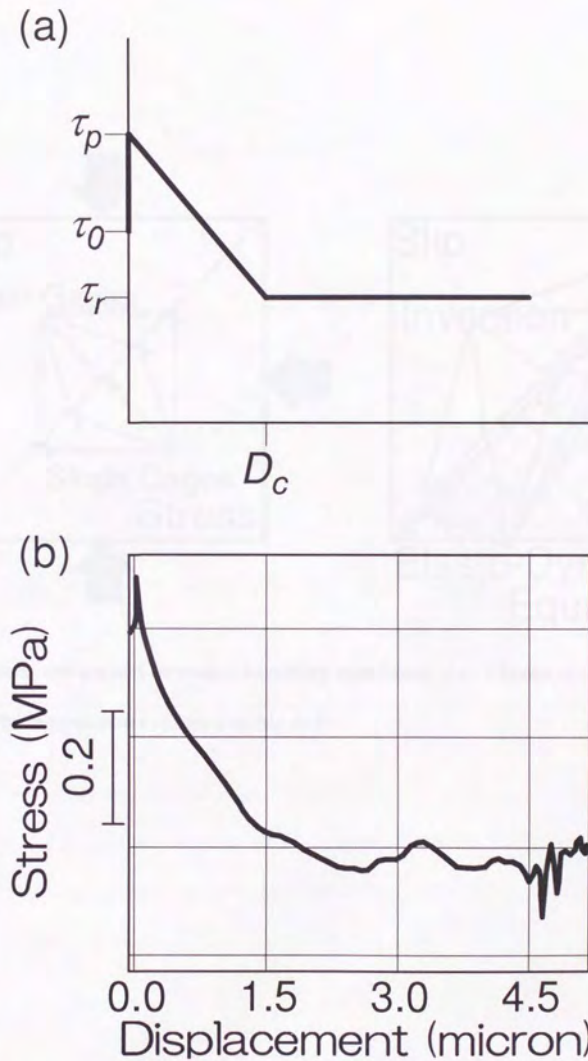
Fig. 1-3. a) Idealized slip-weakening relation showing shear stress as a function of fault displacement.

b) Experimentally observed slip-weakening relation [after Ohnaka *et al.*, 1987].
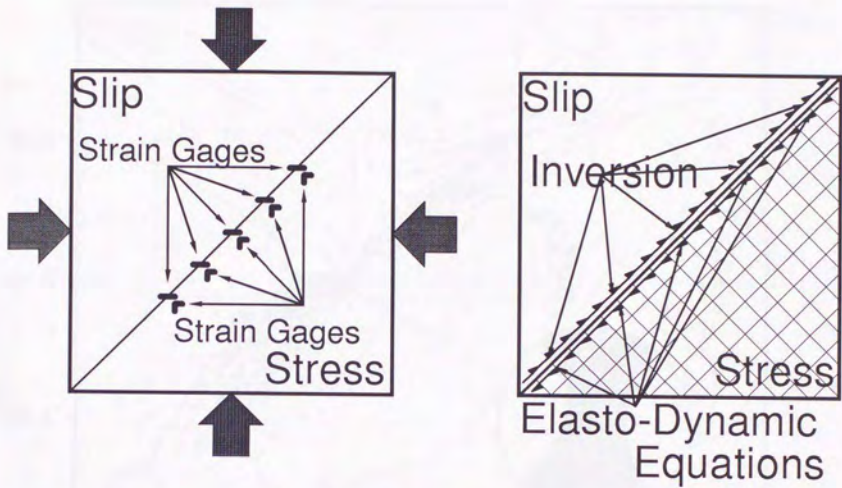
Fig. 1-4. Schematic comparison between a laboratory experiment [*e.g.*, Ohnaka *et al.*, 1987] and the procedure to obtain constitutive relations in this study.
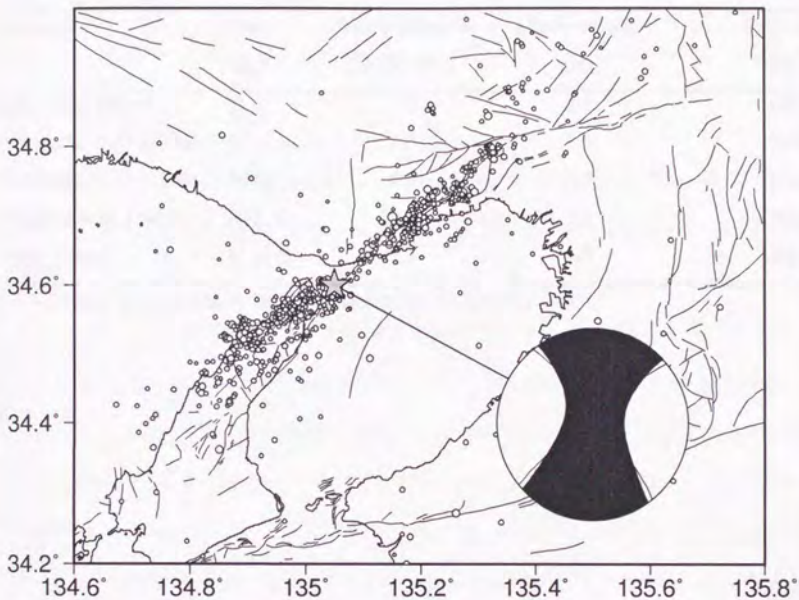
Fig. 1-5 Locations of the mainshock determined by JMA and the aftershocks determined by Japanese University Group for Urgent Joint Observation of the 1995 Hyogo-ken Nanbu Earthquake [Hirata *et al.*, 1996].   The automated CMT solution of ERI [Kawakatsu, 1995] and the active fault traces [The Research Group for Active Faults in Japan, 1991] are also shown.

11

Table 1-1.   Previous result of kinematic analysis of the 1995 Kobe earthquake

Author(s)	Data Used	Seismic Moment ($\times 10^{19}$ Nm)	Maximum Slip (m)	Fault area (km^2)
Ide *et al.* [1996a]	N	2.0	2.8	900
Sekiguchi *et al.* [1996]	N	1.9	1.5	1243
Horikawa *et al.* [1996]	N, G	2.9	2.9	675
Yoshida *et al.* [1996]	N, F, G	2.2	2.8	960
Wald [1996]	N, F, G	2.4	1.7	1200

N: near-field seismogram, F: far-field seismogram, G: geodetic data

Chapter 2

Spatio-Temporal Distribution of Fault Slip

2.1   Method

First, we determine the spatio-temporal distribution of slip on an assumed fault plane by inversion of near-field strong-motion seismograms. Many studies have determined the source process of various earthquakes as spatio-temporal distributions of slip on the fault planes using near-field seismic waves since 1979 Imperial Valley earthquake [Olson and Aspel, 1982; Hartzell and Heaton, 1983]. Various inversion methods have been developed to perform seismic source analysis, and normally some type of flexibility is introduced to express the complex rupture process. Assumed faults are conventionally divided into many subfaults to represent spatial complexity, with the total rupture process being composed of their individual slip histories. To represent temporal complexity, Hartzell and Heaton [1983] allowed subfaults to slip repeatedly in the manner of circular time window propagation from the hypocenter at fixed velocity. Because the timing of each rupture is fixed, this method enables a linear inversion that ensures the uniqueness of the solution. Slightly different approaches of linear inversion are developed by Takeo [1992] and Yoshida [1992]. They expanded the slip-rate function of each subfault by basis functions and determined their coefficients.

These methods generally require numerous parameters and various constraints adopted to perform stable inversion, namely with small model covariance. Therefore, without objective estimation of the weights of these constraints, an objectively unique solution cannot be obtained. Although the method of Hartzell and Heaton [1983] was continuously applied for many large earthquakes, *e.g.*, the 1984 Morgan Hill earthquake [Hartzell and Heaton, 1986], the 1989 Loma

13

Prieta earthquake [Wald *et al.*, 1991], the 1991 Landers earthquake [Wald and Heaton, 1994], the 1994 Northridge earthquake [Wald *et al.*, 1996], and the Kobe earthquake [Wald, 1996] the significance of this objectivity has been almost neglected in these studies.

A useful solution to maintain objectivity under linear constraints on model parameters is constructing a Bayesian model, which consists of a family of parametric models having hyperparameters that correspond to the weights of constraints.   To select a specific model from the family of parametric models, I employ Akaike's Bayesian Information Criterion (ABIC) [Akaike, 1980].   ABIC is based on the entropy maximization principle and has been successfully used in various fields.   Concerning geophysics, Yabuki and Matsu'ura [1992] demonstrated its usefulness by applying it to perform an inversion analysis of geodetic data, while Yoshida [1989] and Yoshida and Koketsu [1990] subsequently applied it to the inversions of seismic source processes.   While they used a nonlinear inversion method in which the uniqueness of solution is difficult to be verified, Ide *et al.* [1996a] adopted ABIC to the linear inversion of Takeo [1992] and Yoshida [1992] to allow the rupture history of an earthquake to be uniquely determined from a statistical standpoint.

Although a subfault discretization system is convenient for the representation of spatial distribution of slip, it has defects (1) that it is not continuous at the subfault boundaries and hence unsuitable for the following FDM calculation, and (2) that the slip-rate function at a point in a subfault is difficult to be determined from the function of whole subfault because it composed of the slip of many different points in the subfault at different rupture time.   A more general representation of slip distribution is expansion by 2-D spatial and temporal basis functions, with the expansion coefficients being unknown parameters.   The spatio-temporal distribution of slip rate $\dot{u}_i(x_1,x_2,t)$ is expanded as,

$$\dot{u}_i(\mathbf{x},t) = \sum a_{ilmn}\phi_l^1(x_1)\phi_m^2(x_2)\psi_n(t), \qquad (2\text{-}1)$$

where a_{ilmn} are the expansion coefficients, and $\phi_l^1(x_1)$, $\phi_m^2(x_2)$, and $\psi_n(t)$ are the basis functions in strike direction, dip direction, and time, respectively.   If one selects a boxcar function as spatial basis function, (2-1) is identical with the conventional subfault discretization system.   In this study, each basis function is a linear B-spline whose shape is triangle and determined by three knots, and hence the slip distribution is continuous everywhere spatially and temporally.   The slip-rate function at a point is easily determined by use of (2-1) with obtained model parameters a_{ilmn}.

The relation between the synthetic displacement at a station and the slip rate distribution $\dot{u}_i(\mathbf{x},t)$ on the fault plane is represented as

$$u_j(\mathbf{x},t) = \iint g_{ij}(\mathbf{x},t;\xi,\tau)\dot{u}_i(\xi,\tau)d\xi d\tau, \tag{2-2}$$

where $g_{ij}(\mathbf{x},t;\xi,\tau)$ is a Green's function representing the jth component of the synthetic displacement when an impulsive slip rate in the ith direction is applied at $\mathbf{x}=\xi$, $t=\tau$ [e.g., Aki and Richards, 1980].   From (2-1) into (2-2), an equation with observed displacement $u_j^o(\mathbf{x},t)$ is obtained as

$$u_j^o(\mathbf{x},t) = \sum a_{ilmn} \iint g_{ij}(\mathbf{x},t;\xi,\tau)\phi_l^1(\xi_1)\phi_m^2(\xi_2)\psi_n(\tau)d\xi d\tau + e_j(\mathbf{x},t), \tag{2-3}$$

where $e_j(\mathbf{x},t)$ is the error between the observed and synthetic displacement.   This equation is rewritten in vector form as

$$\mathbf{d} = \mathbf{Gm} + \mathbf{e}, \tag{2-4}$$

where $\mathbf{d}$, $\mathbf{m}$, and $\mathbf{e}$ are the data vector composed of sampled data $u_j^o(\mathbf{x},t)$, the parameter vector of a_{ilmn}, and the error vector of $e_j(\mathbf{x},t)$, respectively. $\mathbf{G}$ is an N, the number of data, x M, the number of parameters, matrix obtained after calculating integration in (2-3) and sampling corresponding to $\mathbf{d}$.

15

It should be noted that the error vector e contains measurement errors and modeling errors, *e.g.*, inaccuracy of (1) the employed Green's functions and (2) assumption of the fault plane geometry. Although it cannot be assured, for simplicity, error e is assumed to be Gaussian with zero mean and covariance $\sigma^2 I$, where I is an identity matrix.   From this assumption and the vector from of observation equation (2-4), a stochastic model that relates the data d with the model parameter m is formulated as

$$p(\mathbf{d}|\mathbf{m};\sigma^2) = (2\pi\sigma^2)^{-N/2} \exp\left[-\frac{1}{2\sigma^2} \|\mathbf{d} - \mathbf{Gm}\|^2 \right], \tag{2-5}$$

which is a likelihood function of m and σ^2 for given d.   Without prior information about m, maximizing (2-5) yields the appropriate values of m and data variance σ^2.

However, the estimate of m by minimizing (2-5) alone usually has large model covariances and shows quite irregular slip distribution.   Therefore, I introduce two types of smoothing constraints as prior information of Bayesian modeling: the temporal constraint and the spatial constraint.   For the temporal constraint, the smoothness of the slip-rate function is assumed as

$$\mathbf{D}_1\mathbf{m} = \mathbf{e}_1, \tag{2-6}$$

where $\mathbf{D}_1$ is a N_1 x M matrix which is the finite difference operator of partial derivative by time, and $\mathbf{e}_1$ is error vector.   For the spatial constraint, the smoothness of the spatial distribution of total slip is introduced by a Laplacian finite difference operator; *i.e.*,

$$\mathbf{D}_2\mathbf{m} = \mathbf{e}_2, \tag{2-7}$$

where $\mathbf{D}_2$ and $\mathbf{e}_2$ are N_2 x M matrix and error vector, respectively.   It should be noted that this constraint does not affect the instantaneous smoothness of the spatial slip distribution.   As with e, error vector $\mathbf{e}_1$ and $\mathbf{e}_2$ are assumed as Gaussian with zero mean and covariance $\sigma_1^2 I$ and $\sigma_2^2 I$,

respectively.

These temporal and spatial smoothing constraints, when they are regarded as prior information associated with the model parameters, can be formulated as the following probability density function (PDF):

$$p(\mathbf{m}; \sigma_1^2, \sigma_2^2) = (2\pi\sigma_1^2)^{-N_1'/2}(2\pi\sigma_2^2)^{-N_2'}\|\Lambda_1\|^{1/2}\|\Lambda_2\|^{1/2}$$
$$\times \exp\left(-\frac{1}{2\sigma_1^2}\|\mathbf{D}_1\mathbf{m}\|^2\right)\exp\left(-\frac{1}{2\sigma_2^2}\|\mathbf{D}_2\mathbf{m}\|^2\right), \tag{2-8}$$

where N_1' and N_2' are the rank of $\mathbf{D}_1{}^t\mathbf{D}_1$ and $\mathbf{D}_2{}^t\mathbf{D}_2$, respectively, and $\|\Lambda_1\|$ and $\|\Lambda_2\|$ represent the absolute value of the product of nonzero eigenvalues of $\mathbf{D}_1{}^t\mathbf{D}_1$ and $\mathbf{D}_2{}^t\mathbf{D}_2$, respectively. Superscript t indicates the transposition of the matrix.   As formulated in (2-8), σ_1^2 and σ_2^2 control the prior distribution of $\mathbf{m}$ and then are regarded as hyperparameters.   As σ_1^2 becomes large, the temporal change of slip-rate becomes rapid, namely rough slip-rate functions, and correspondingly, as σ_2^2 becomes large, the total spatial distribution of slip becomes rough.

Application of Bayes theorem enables the prior information $p(\mathbf{m}; \sigma_1^2, \sigma_2^2)$ in (2-8) to be incorporated with the likelihood function $p(\mathbf{d}|\mathbf{m}; \sigma^2)$ in (2-5), resulting in a Bayesian model having a posterior PDF with three hyperparameters σ^2, σ_1^2 and σ_2^2; *i.e.*,

$$p(\mathbf{m}; \sigma_1^2, \sigma_2^2, \sigma^2|\mathbf{d}) = Cp(\mathbf{d}|\mathbf{m}; \sigma^2)p(\mathbf{m}; \sigma_1^2, \sigma_2^2), \tag{2-9}$$

where C is introduced as a normalizing factor whose definition is tailored such that $p(\mathbf{m}; \sigma_1^2, \sigma_2^2, \sigma^2|\mathbf{d})$ is reduced to unity following integration with respect to $\mathbf{m}$.   Then substituting (2-5) and (2-8) into (2-9), the posterior PDF is rewritten as,

$$p(\mathbf{m}; \alpha_1^2, \alpha_2^2, \sigma^2 | \mathbf{d}) = C(2\pi\sigma^2)^{-(N+N_1'+N_2')/2} (\alpha_1^2)^{N_1'/2} (\alpha_2^2)^{N_2'/2}$$
$$\times \|\Lambda_1\|^{1/2} \|\Lambda_2\|^{1/2} \exp\left[-\frac{1}{2\sigma^2} s(\mathbf{m})\right], \tag{2-10}$$

where

$$s(\mathbf{m}) = \|\mathbf{d} - \mathbf{Gm}\|^2 + \alpha_1^2 \|\mathbf{D}_1\mathbf{m}\|^2 + \alpha_2^2 \|\mathbf{D}_2\mathbf{m}\|^2, \tag{2-11}$$

and $\alpha_1^2 = \sigma^2 / \sigma_1^2$ and $\alpha_2^2 = \sigma^2 / \sigma_2^2$ are new hyperparameters introduced instead of σ_1^2 and σ_2^2. If hyperparameters α_1^2 and α_2^2 are fixed, maximizing (2-10) is formally transformed into a damped least-squares problem that minimizes s($\mathbf{m}$).   As such, the best estimates of model parameter $\mathbf{m}^*$ and their covariance matrix C, are given for any combination of α_1^2 and α_2^2, using the method described by Jackson and Matsu'ura [1985], thereby obtaining,

$$\mathbf{m}^* = \left(\mathbf{G}^t\mathbf{G} + \alpha_1^2\mathbf{D}_1{}^t\mathbf{D}_1 + \alpha_2^2\mathbf{D}_2{}^t\mathbf{D}_2\right)^{-1}\mathbf{G}^t\mathbf{d}, \tag{2-12}$$

$$\mathbf{C} = \sigma^2 \left(\mathbf{G}^t\mathbf{G} + \alpha_1^2\mathbf{D}_1{}^t\mathbf{D}_1 + \alpha_2^2\mathbf{D}_2{}^t\mathbf{D}_2\right)^{-1}, \tag{2-13}$$

The best estimates of these hyperparameters are calculated by minimizing Akaike's Bayesian Information Criterion (ABIC) [Akaike, 1980], which is formulated on the principle of maximizing entropy and defined as minus twice the marginal likelihood, whose definition is,

$$L(\sigma^2, \sigma_1^2, \sigma_2^2) = \int p(\mathbf{d}|\mathbf{m}; \sigma^2) p(\mathbf{m}; \sigma_1^2, \sigma_2^2) d\mathbf{m}. \tag{2-14}$$

The minimum of ABIC indicates that the information of data is necessarily and sufficiently used to determine the estimates of model parameters.   After substituting the likelihood function (2-5) and the prior information (2-8) into (2-14), changing σ_1^2 and σ_2^2 into α_1^2 and α_2^2, integration with respect to $\mathbf{m}$ gives

$$L(\sigma^2, \alpha_1^2, \alpha_2^2) = (2\pi\sigma^2)^{-(N+N_1'+N_2')/2} (\alpha_1^2)^{N_1'/2} (\alpha_2^2)^{N_2'/2}$$
$$\times \|\Lambda_1\|^{1/2} \|\Lambda_2\|^{1/2} \|G^tG + \alpha_1^2 D_1'D_1 + \alpha_2^2 D_2'D_2\|^{-1/2} \tag{2-15}$$
$$\times \exp\left[-\frac{1}{2\sigma^2} s(m^*)\right],$$

where m^* is the best estimate of model parameters for fixed α_1^2 and α_2^2. Since the optimum values

of the data variance σ^2 minimizes the ABIC, namely it maximizes $L(\sigma^2, \alpha_1^2, \alpha_2^2)$, partial derivative

of $L(\sigma^2, \alpha_1^2, \alpha_2^2)$ by σ^2 must be zero for the minimum ABIC. Thus, the optimum value of σ^2 is

determined as

$$\sigma^2 = s(m^*) / (N + N_1' + N_2' - M). \tag{2-16}$$

Then, using (2-16) and the marginal likelihood (2-15), the ABIC is written as

$$\text{ABIC}(\alpha_1^2, \alpha_2^2) = (N + N_1' + N_2' - M) \log s(m^*) - N_1' \log \alpha_1^2 - N_2' \log \alpha_2^2$$
$$+ \log \|G^tG + \alpha_1^2 D_1'D_1 + \alpha_2^2 D_2'D_2\|. \tag{2-17}$$

In the calculation, the best estimate of model parameter m^* is first obtained using particular

values of α_1^2 and α_2^2 and (2-12). In parallel, the covariance of the model parameter C and σ^2 for

this m^* are respectively obtained using (2-13) and (2-16). Equation (2-17) then gives the ABIC by

numerical computation using resultant m^*, α_1^2, and α_2^2. The values of α_1^2 and α_2^2 are

subsequently varied, and this procedure is repeated until the minimum ABIC value is found. After

determining the set of α_1^2 and α_2^2 minimizing the ABIC, m^* previously obtained with these values

and (2-12) turns into the optimum model parameter m^* that construct the spatio-temporal

distribution of fault slip.

2-2   Preparation for Inversion

The Japan Meteorological Agency (JMA) determined the location of the mainshock hypocenter

to be 34.61° N and 135.04° E at a depth 14.3 km.   Fig. 2-1 shows its location and the distribution of

aftershocks as determined by the Japanese University Group for Urgent Joint Observation of the 1995

Hyogo-ken Nanbu Earthquake [Hirata et al., 1996], where the aftershock distribution from 27

January to 9 February forms an almost vertical plane striking along N52° E.   Although this period is

10 days after the mainshock, and by 27 January there had been an obvious migration of aftershock

toward the northeast, this distribution was nevertheless used because its precise location determined

following installation of a dense network of seismometers right above the source area.

To determine a spatio-temporal distribution of fault slip, I initially arrange an assumed fault plane

in the source region, and determine a spatio-temporal slip distribution on the plane.   The fault plane

is assumed based on the observed aftershock distribution and the CMT solution, whose focal

mechanism is also shown in Fig. 1-5.   One of two nodal planes of the best double couple solution of

the CMT shows a strike direction that corresponds with the lineation of the aftershock distribution.

Therefore, the assumed fault plane strikes along N232° E and has a dip angle of 85° in a northwest

direction, being inclined only 5° away from vertical.

Some fault planes having different strike and dip angles are considered in the analyses of

Horikawa et al. [1996], Yoshida et al. [1996], and Wald [1996] to be consistent with the geodetic

observation, and in the analysis of Sekiguchi et al. [1996] to explain the particle motions of quite

near-field strong-motion seismograms in the northeastern area of the source region (Kobe area).

Although in the southwest area of the source region (Awaji area), they used vertical or slightly

dipping fault planes to the southeast, a recent precise determination of the aftershock locations

[Nakamura and Ando, 1996] shows that the aftershock distribution shows almost the same dipping

angle of 85° to the northwest in both Kobe area and northern Awaji area.   In the present study, only

20

strong-motion data of relatively low frequency is used, hence the mislocation of fault plane is neglected after appropriate correction of travel time discussed later.   The length and the width of the fault plane are 50 km and 20 km, which covers the whole source extent as shown by the detailed analysis of Ide *et al.* [1996a].   By analysis using rough wide fault system, Ide *et al.* [1996a] concluded that few ruptures occurred out of this area though there are many aftershocks because of the aftershock migration during 10 days after the mainshock.

To expand the spatio-temporal distribution on the assumed fault using linear B-spline functions, the knots of the spline function are arranged in the 3-D source volume, a 2-D fault plane and a time axis (Fig. 2-2).   The front view (Fig. 2-2d) shows a spatial distribution of knots whose interval is set at 2.5 km, and the top (Fig. 2-2b) and the side (Fig. 2-2e) views show the locations of knots in the time direction with an interval of 0.6 s.   These values are determined mainly by computational limitations and much smaller intervals are desirable for more detailed source representation.   To save computational costs, knots are activated for each point on the fault plane after an imaginary rupture front with a propagation velocity of 3.0 km/s reaches there.   This rupture velocity limits only the initiation time of rupture and the local rupture velocity between neighboring knots, and a proper choice of the expansion coefficients enables a faster or a slower rupture than this velocity.   The numbers of the basis functions in strike, dip, and time direction are 19, 8, and 11 respectively; the total number necessary to represent slip of a specific direction is then 1672.   Since this earthquake has almost pure right-lateral strike-having rake angle of 180° as shown in CMT solution (Fig. 1-5), two directions of slip on this fault plane are assumed: the rake angles of 135° (right-lateral strike-slip with thrust slip component) and 225° (right-lateral strike-slip with normal slip component), and slip at each point is represents by the composition of these slip vectors.   Slip distribution in one direction is expanded by 1672 basis functions, hence the total number of basis functions and expansion coefficients is 3344.   By constraining expansion coefficients to be positive in the following inversion,

slip direction at any point on the fault plane is limited between 135° and 225°.

The original data are strong-motion seismograms recorded by acceleration seismometers operated at 18 JMA stations located less than 150 km away from the hypocenter (Fig. 2-3, Table 2-1).   Eight stations provided seismograms from A-type units that have a flat frequency response from 0.01 to 10 Hz [Katsumata, 1989].   Each seismogram furnished three components of acceleration data, namely, up-down (UD), north-south (NS), and east-west (EW) for a total of 24 components.   The UD component of Kobe station (KOB) located 1 km northwest of the assumed fault plane was eliminated from the data set because this component suffers the effect of fault mislocation and is almost independent of the whole rupture process, while the horizontal components are well associated with the source process near the hypocenter as well as the fault area near KOB station [Ide *et al.*, 1996b]. The other 10 stations provided seismograms, each with the same acceleration component, from new B-type units that have a flat frequency response from 0 to 8.2 Hz [Yoshida and Yokota, 1994]. Eliminating the seismograms that is affected by some recording trouble, 22 of 30 components of acceleration data are selected (Table 2-1).   Therefore, 45 seismograms were processed into displacement data by integrating twice and then band-pass filtered from 0.025 to 0.5 Hz to remove low-frequency noise amplified by the integrations.   Use of a 0.2 s sampling interval and a 50 s period extracted from each of the 45 displacement records provided 11,295 data points.   Each data point was equally weighted in the inversion analysis so as to fit the larger data values better.

The Green's function in (2-2) is calculated using a point source of impulsive slip rate for each slip direction at each calculation point arranged at 1 km interval on the assumed fault plane by the discrete wavenumber method of Bouchon [1981] in which the reflection-transmission matrices of Kennet and Kerry [1979] are used.   The effect of anelasticity is also introduced by the use of complex velocities [Takeo, 1985].   The interval of 1 km is fine enough to be assumed as a point source because the rupture propagation at this distance is about 0.3-0.4 s and comparable to the duration of the

22

discretized version of a delta function at a sampling interval of 0.2 s.

For the structure of seismic velocities in the analysis region of western Japan, a horizontal crustal structure is assumed based on the P-wave velocity structure deduced from an explosion survey performed along a line passing right through Kobe and Awaji Island [Aoki and Muramatsu, 1973]. The S-wave velocity structure is estimated from P-wave velocities assuming a Poisson's ratio of 0.25, and ρ, Q_p, are Q_s are tailored to be appropriate for the velocity and depth of each layer (Table 2-2). The fact that the calculated and observed travel times of P-wave and S-P times agree well as shown in Fig. 2-4 supports the appropriateness of this structure.   Even small errors in timing may generate large misfits in the waveform analysis, therefore the time alignments are applied to all combination of Green's functions and data.   The P-wave arrival times are aligned for the UD component, while S-wave arrival times were similarly aligned for the horizontal EW and NS components.   After the same band-pass filtering as data and convolution with temporal basis function, the surface integral in (2-3) is performed numerically at 1 km sampling interval to write observation equations in matrix style.

2-3   Inversion Results

To solve (2-12) with a positivity constraint on the model parameters, I employed the non-negative least-squares (NNLS) algorithm of Lawson and Hanson [1974].   Fig. 2-5 shows the resultant values of ABIC obtained by the inversions with various values of hyperparameters α_1^2 and α_2^2.   Since the absolute value of ABIC is meaningless, it shows only the differences from the minimum ABIC, which occurs at $\alpha_1^2 = 0.5$ and $\alpha_2^2 = 0.5$, being the optimal set.   Fig. 2-6 shows the spatial distribution of total slip and its direction at $\alpha_1^2 = 0.5$ and $\alpha_2^2 = 0.5$, while Fig. 2-7 shows the corresponding slip-rate functions at 10 selected points on the fault plane.

This solution has the same following characteristics as the previous kinematic models shown in Table 1-1. The area of large slip extends near the hypocenter and shallow southwest part of the fault plane, where the maximum slip of 2 m occurred. This large shallow slip corresponds to the observed fault offsets of about 1 m along the Nojima fault [Nakata and Yomogida, 1995; Awata *et al.*, 1995]. The total seismic moment is calculated as 1.9×10^{19} Nm, comparable as the previous works (Table 1-1). Relatively large thrust component exists near the hypocenter, beneath Akashi strait, suggesting the rupture initiation mechanism may be different from overall mechanism of this earthquake. Thrust slip beneath Akashi strait was reported by Hashimoto *et al.* [1996] from the analysis of geodetic data.

The shapes of slip-rate functions differ from place to place in the fault plane (Fig. 2-7). The duration of each slip-rate function, rise time, at shallow depth (**a-d**) are about 5 s and its shape resembles a boxcar function, whereas the rise time is less than 3 s (**f, i**), and the shape resembles a triangle (**e, h**) at deeper depth. The long duration of the slip-rate function at shallow depth has been reported by Ide *et al.* [1996a], Sekiguchi *et al.* [1996], and Wald [1996] though they could not separate the rise time at each point of the fault plane and the effect of rupture propagation within each subfault from the slip-rate functions. In this study, these two effects can be considered separately using the expansion of slip distribution by basis functions if the data supply enough information. However, the information seems not to be sufficient to successfully separate them due to the limited frequency band, up to 0.5 Hz, of data. The highest frequency of 0.5 Hz suggests the upper spatial resolution of 5-6 km, assuming the characteristic rupture velocity of 2.5 - 3.0 km/s. As a consequence, the obtained slip distribution and slip-rate functions are quite similar to the previous result obtained using 5 km subfaults [Ide *et al.*, 1996a].

Fig. 2-8 depicts the determined rupture history of this earthquake as slip-rate distribution at each 1 s time interval. Rupture begins from the hypocenter and propagates mainly toward the surface in

the northeast direction from 0 to 3 s (phase **A**), and has a large thrust component.   This unilateral

rupture phase is confirmed independently by other studies; Ellsworth [1995] indicated that the initial

rupture propagation directs towards the northeast direction by the analysis of the initial parts of

strong-motion seismograms of JMA, while Shibazaki [1996, personal communication] also supported

the initial northeastward directivity by the analysis using the empirical Green's function method.

The rupture propagation in this direction soon weakens (5 s), whereas the other southwesterly

propagation begins at 3 s and continues progressing upward with an increasing slip velocity (phase **B**).

Slip rate reaches a maximum (0.8 m/s) at the surface corresponding to the location of the Nojima

fault (8 s).   After northeastern rupture propagation of phase **A** weakens, the rupture to the northeast

continues until 11 s after the origin of the mainshock (phase **C**).   The rupture in phase **C** rupture is

characterized by highly irregular propagation with small total slip, suggesting that a complex crustal

structure exists in this region that corresponds with the complexity of active fault distribution there

(Fig. 1-5).   The rupture in phase **C** is deeper than that in phase **B**, being consistent with the fact that

there is no surface fault rupture in Kobe region.

As summarized by Heaton [1990], many recent studies of earthquake found the rise times to be

much smaller than total rupture duration.   This is unexpected in the conventional dynamic crack

model [Madariaga, 1976] in which slip continues at the center of the crack until stopping information

reaches there from the crack tip.   The view that emerges from these studies is that an earthquake

consists of a slip-pulse, a propagating band of slip, whose duration is not controlled by fault

dimensions [Heaton, 1990].   Fig. 2-8 also shows such slip-pulse propagation, prominent at 4 s and 9

s.   Although the assumed propagating knots distribution of the basis function (Fig. 2-2) inherently

produces a slip-pulse distribution, the slip-rate functions determined by inversion indicate that the

whole rupture is well constrained within the assumed time window (Fig. 2-7), and the width of the

obtained slip-pulse (about 10 km, Fig. 2-8) is smaller than those of the inherent time window (21.6

km, Fig. 2-2b).   Therefore these slip-pulses are not inherent and are well-determined by the waveform inversion.

Fig. 2-9 compares the observed and calculated displacement records, in which the correlation between the two traces is quite good for nearly all components.   Note that the theoretical model simulates the large-amplitude waves at the KOB (Kobe) station as well as other small-amplitude waves.   The lack of agreement in the records of the OSA (Osaka) station is probably because the station is located on thick alluvial layers: a local geological structure that is not accounted for in the employed Green's functions.   Nevertheless, the long-period components of these records are well explained by the model.
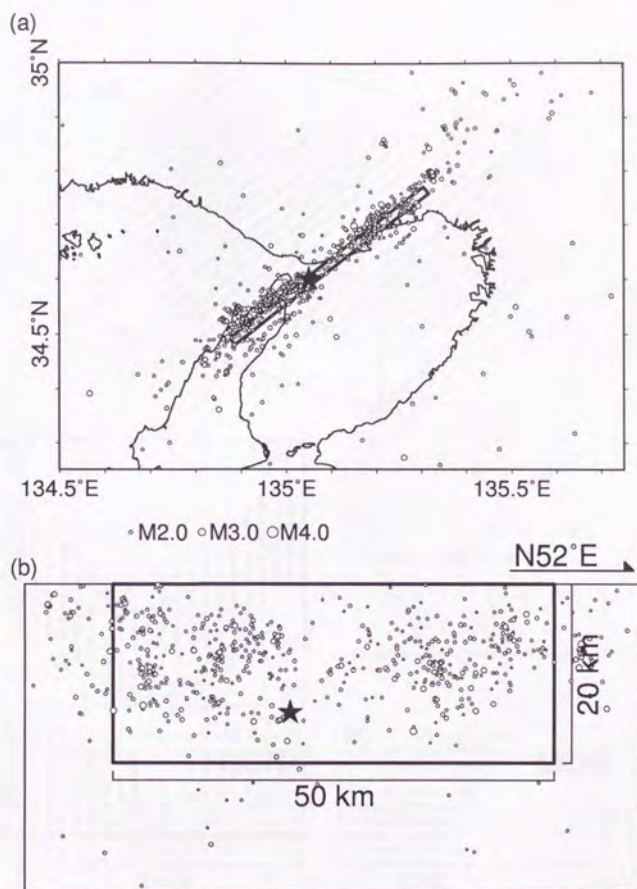
Fig. 2-1 (a) Locations of aftershock determined by Japanese University Group for Urgent Joint Observation of the 1995 Hyogo-ken Nanbu Earthquake [Hirata *et al.*, 1996].   Magnitude sizes are as indicated.   The mainshock location is also shown by a star.   The rectangle represents the assumed fault plane.   (b) Same as (a) projected to the assumed fault plane.   A triangle shows the location of KOB (Kobe) station of JMA.

27
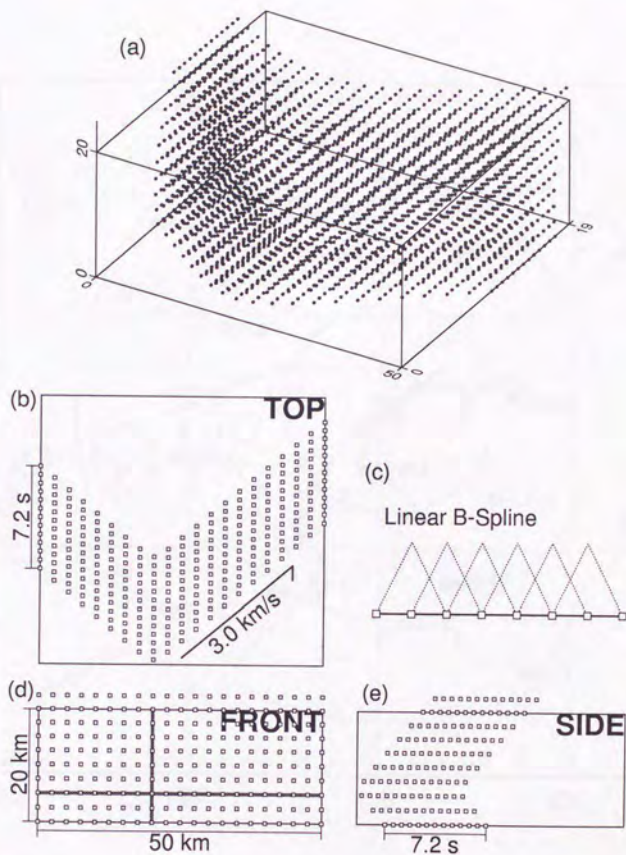
Fig. 2-2 (a) The knots distribution of linear B-spline functions in the present study in 3-D source volume spanned by the assumed fault plane and the time axis.   (b) The distribution on the plane shown in (d) by a horizontal gray line.   (c) The shape of linear B-spline functions with knots distribution.   (d) The front view of (a).   Two horizontal and vertical lines show the projected plane of (b) and (e), respectively.   (e) The distribution of knots on the plane shown in (d) by a vertical gray line.

28
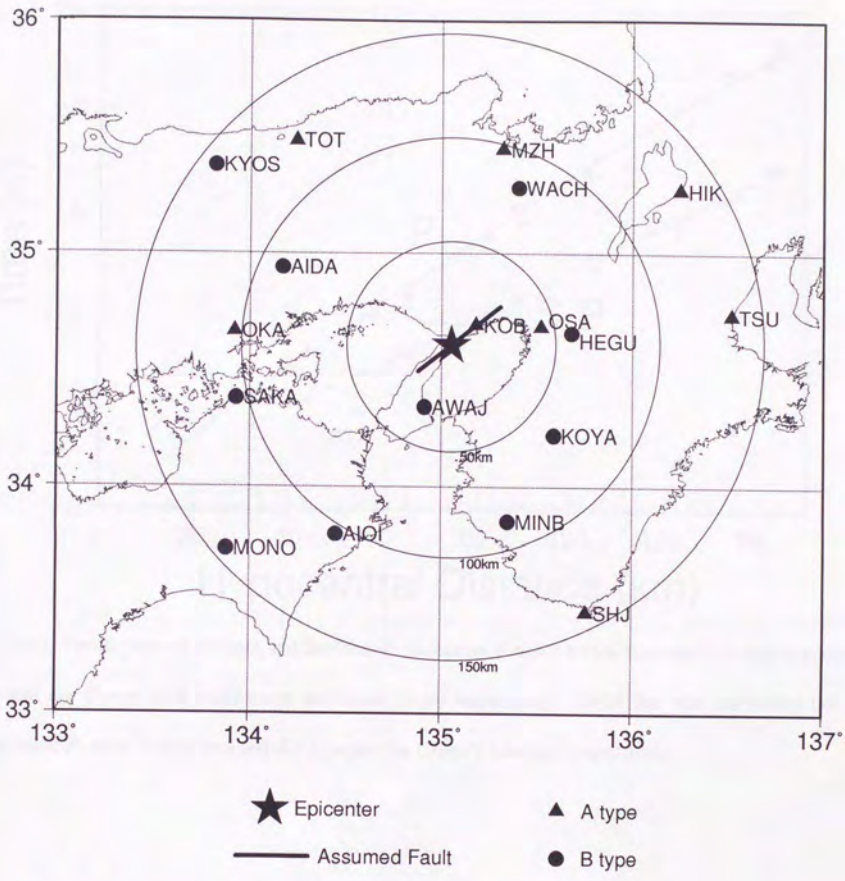
Fig. 2-3 Location map of JMA strong-motion stations used in the analysis.
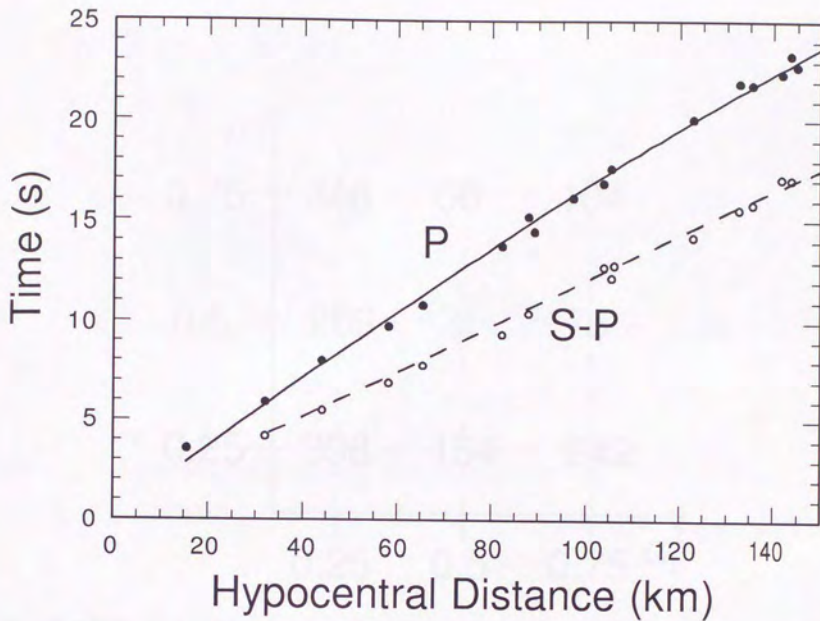
Fig. 2-4 Travel times of the data and the Green's functions. *P*-wave arrival time and *S-P* time at each station are shown by a solid circle and open circle, respectively.   Solid line and the dotted line represent *P*-wave arrival time and *S-P* time for the Green's function, respectively.

$$
\begin{array}{c}
\alpha_2^2 \\
0.75 \quad 346 \quad 66 \quad 104 \\
0.5 \quad 259 \quad \oplus \quad 75 \\
0.25 \quad 398 \quad 164 \quad 242 \\
0.25 \quad 0.5 \quad 0.75 \quad \alpha_1^2
\end{array}
$$
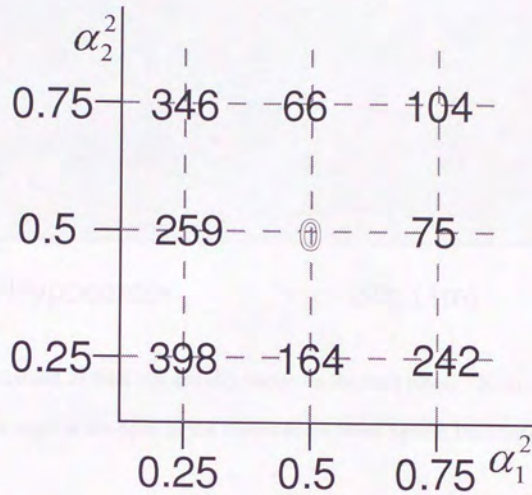
Fig. 2-5 ABIC values in the inversion analysis plotted in the α_1^2 - α_2^2 plane.   The difference from the minimum ($\alpha_1^2 = 0.5$, $\alpha_2^2 = 0.5$) are shown.

☆ Hypocenter　　　　　⟶ Slip (1m)
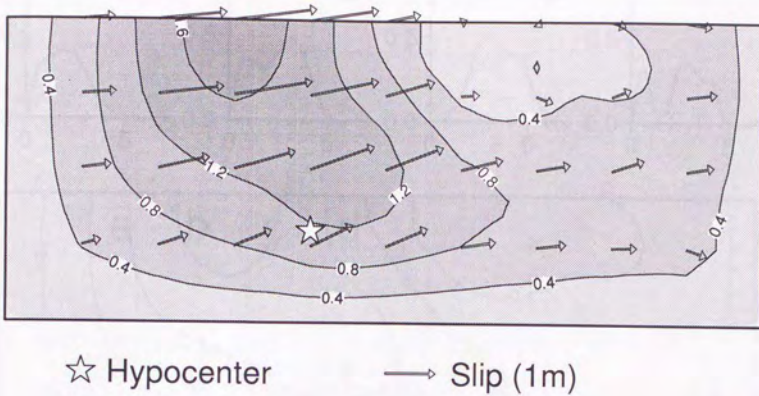
Fig. 2-6 The distribution of total slip and slip vector on the fault plane.　Each vector represents the slip magnitude and angle at the point of the northwestern block against the southeastern block.
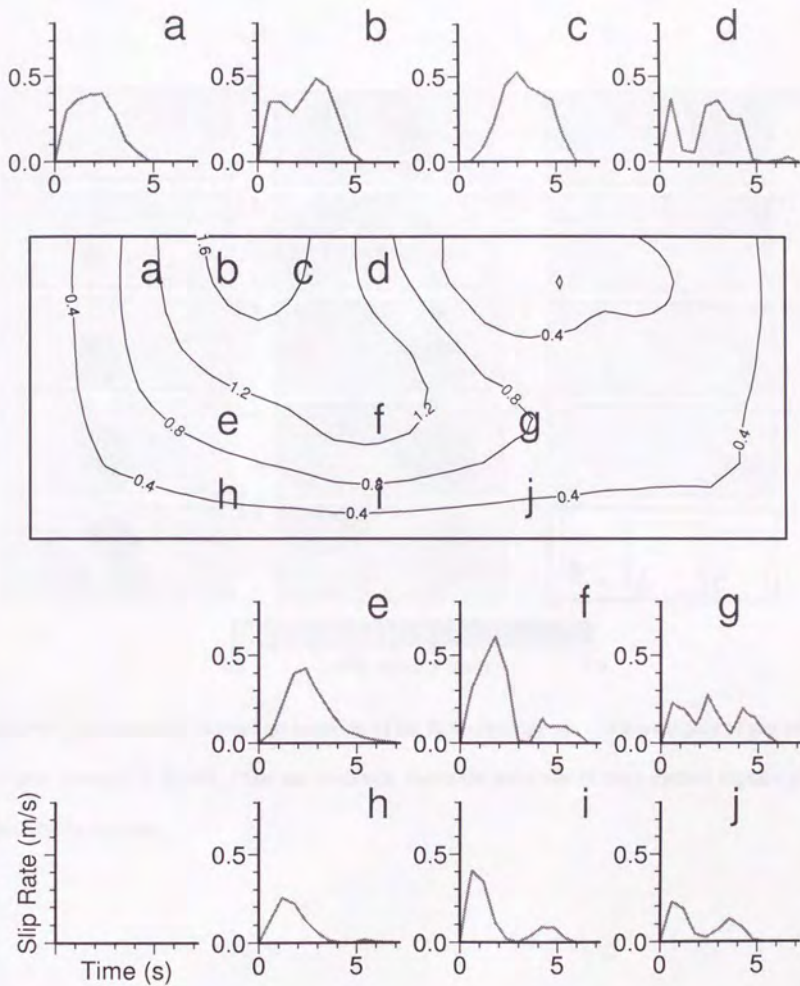
Fig. 2-7 The slip-rate functions at ten selected points shown by **a-j** in the slip distribution.   Each slip-rate function shows change of slip rate within 7.2 s time window after the arrival of an imaginary rupture.
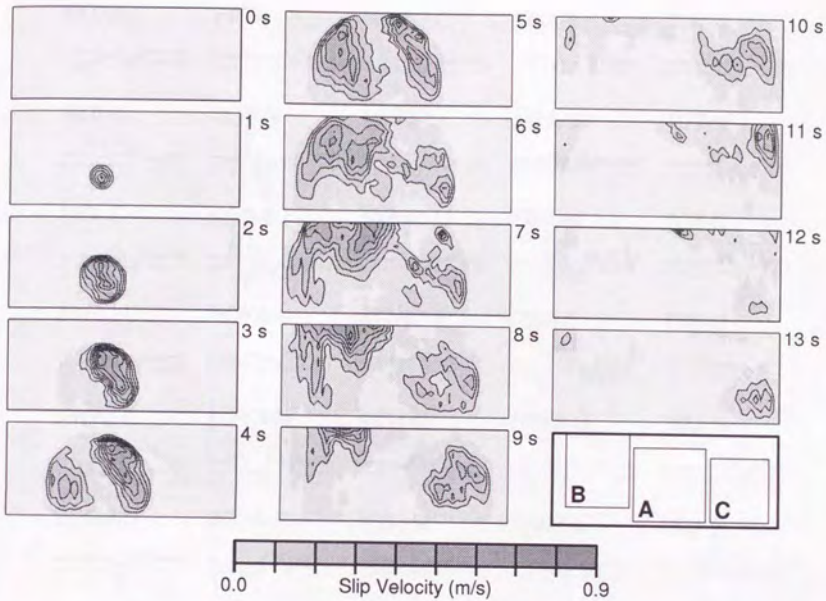
Fig. 2-8 The histories of rupture propagation of the Kobe earthquake.   The amplitude of slip rate at 1 s time intervals is shown.   The last rectangle shows the locations of three distinct rupture phase discussed in the text.
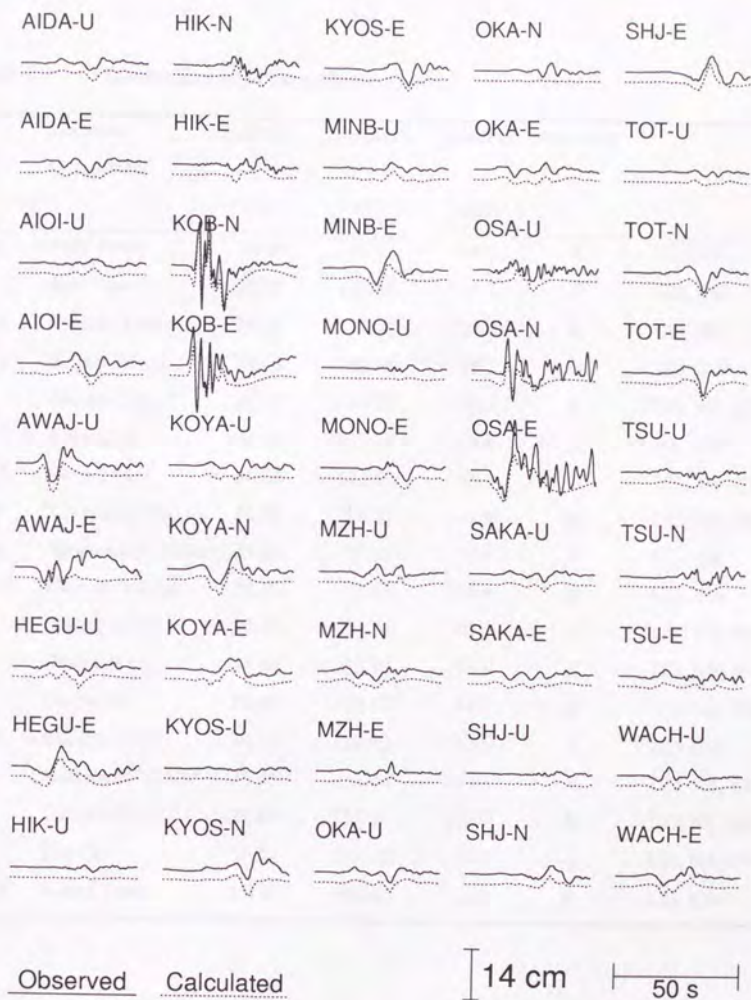
Fig. 2-9 Observed (solid lines) and calculated displacement (dotted lines) for the kinematic source model. Station code, component, and start time of the record from the hypocentral time (s) are respectively indicated on the top of each set of trace.

Table 2-1   Station list used in the analysis.

Code	Location Component	Latitude (°)	Longitude (°)	Distance (km)	Instrument	
AIDA	Aida Town	34.94	134.17	89.0	B	UD, EW
AIOI	Aioi Town	33.79	134.45	105.3	B	UD, EW
AWAJ	Sumoto Town	34.34	134.91	32.0	B	UD, EW
HEGU	Heguri Town	34.65	135.68	58.1	B	UD, EW
HIK	Hikone City	35.27	136.25	132.6	A	UD, NS, EW
KOB	Kobe City	34.69	135.18	15.4	A	NS, EW
KOYA	Koya Town	34.22	135.59	65.3	B	UD, NS, EW
KYOS	Kurayoshi City	35.38	133.82	141.6	B	UD, NS, EW
MINB	Minabekawa Village	33.85	135.35	87.7	B	UD, EW
MONO	Monobe Village	33.73	133.88	144.9	B	UD, EW
MZH	Maizuru City	35.45	135.32	97.2	A	UD, NS, EW
OKA	Okayama City	34.66	133.92	103.8	A	UD, NS, EW
OSA	Osaka City	34.68	135.52	44.0	A	UD, NS, EW
SAKA	Sakaide City	34.37	133.93	105.9	B	UD, EW
SHJ	Kushimoto Town	33.45	135.76	143.6	A	UD, NS, EW
TOT	Tottori City	35.49	134.24	122.9	A	UD, NS, EW
TSU	Tsu City	34.73	136.52	135.5	A	UD, NS, EW
WACH	Wachi Town	35.28	135.40	82.2	B	UD, EW

Table 2-2   Parameters of the velocity structure used in the inversion analysis.

Layer No.	V_p (km/s)	V_s (km/s)	ρ (g/cm^3)	h (km)	Q_p	Q_s
1	5.5	3.2	2.5	0.0	400	200
2	6.0	3.5	2.7	3.0	600	300
3	6.6	3.8	3.0	22.0	800	400
4	7.8	4.5	3.2	31.0	1000	500

Chapter 3

Stress Distribution and Constitutive Relations

3-1   Method

To determine the stress distribution on the fault plane from the spatio-temporal distribution obtained by inversion, I employed a finite difference method (FDM) [*e.g.*, Mikumo *et al.*, 1987] with the   slip distribution as a boundary condition.   The equations of motion,

$$\rho \ddot{u}_i = \tau_{ij,j} \tag{3-1}$$

and Hooke's law,

$$\tau_{ij} = \lambda u_{k,k} \delta_{ij} + \mu(u_{i,j} + u_{j,i}) \tag{3-2}$$

are solved in 3-D elastic body surrounded by a fault plane, a free surface, and the four other rigid boundaries. u_i and τ_{ij} represent the i component of the displacement vector and the ij component of the stress tensor, respectively, and $,j$ means partial derivative in j direction. ρ is density, λ and μ are elastic coefficients, and δ_{ij} is a Kronecker's delta.   Since the initial values of the stress components are unknown and only the difference from the initial state is important to solve (3-1) and (3-2), u_i and τ_{ij} are regarded as the differences from the initial values before the rupture initiation (t = 0)   Fig. 3-1 illustrates this model configuration with axis orientation: x, y, and z axes are in strike direction, perpendicular to the fault plane, vertical, respectively.   For simplicity a vertical fault plane is adopted in FDM calculation, although the slip distribution is determined on a slightly dipping (dip angle 85° in northwest) fault plane.   Combining (3-1) and (3-2) yields the following set of wave

38

equations:

$$\ddot{u}_x = \frac{\lambda+\mu}{\rho}\frac{\partial^2 u_x}{\partial x^2} + \frac{\mu}{\rho}\nabla^2 u_x + \frac{\lambda+\mu}{\rho}\frac{\partial^2 u_y}{\partial x\partial y} + \frac{\lambda+\mu}{\rho}\frac{\partial^2 u_z}{\partial x\partial z}$$

$$\ddot{u}_y = \frac{\lambda+\mu}{\rho}\frac{\partial^2 u_x}{\partial x\partial y} + \frac{\lambda+\mu}{\rho}\frac{\partial^2 u_y}{\partial y^2} + \frac{\mu}{\rho}\nabla^2 u_y + \frac{\lambda+\mu}{\rho}\frac{\partial^2 u_z}{\partial y\partial z} \qquad (3\text{-}3)$$

$$\ddot{u}_z = \frac{\lambda+\mu}{\rho}\frac{\partial^2 u_x}{\partial x\partial z} + \frac{\lambda+\mu}{\rho}\frac{\partial^2 u_y}{\partial x\partial z} + \frac{\lambda+\mu}{\rho}\frac{\partial^2 u_z}{\partial z^2} + \frac{\mu}{\rho}\nabla^2 u_x .$$

They are rewritten as the finite difference manner:

$$
\begin{aligned}
u_x^{\,i,j,k,l+1} &= 2u_x^{\,i,j,k,l} - u_x^{\,i,j,k,l-1} + \frac{\lambda+2\mu}{\rho}\frac{\Delta t^2}{\Delta x^2}\left(u_x^{\,i+1,j,k,l} - u_x^{\,i,j,k,l} + u_x^{\,i-1,j,k,l}\right) \\
&+ \frac{\mu}{\rho}\frac{\Delta t^2}{\Delta y^2}\left(u_x^{\,i,j+1,k,l} - u_x^{\,i,j,k,l} + u_x^{\,i,j-1,k,l}\right) + \frac{\mu}{\rho}\frac{\Delta t^2}{\Delta z^2}\left(u_x^{\,i,j,k+1,l} - u_x^{\,i,j,k,l} + u_x^{\,i,j,k-1,l}\right) \\
&+ \frac{\lambda+\mu}{4\rho}\frac{\Delta t^2}{\Delta x\Delta y}\left(u_y^{\,i+1,j+1,k,l} - u_y^{\,i+1,j-1,k,l} - u_y^{\,i-1,j+1,k,l} + u_y^{\,i-1,j-1,k,l}\right) \\
&+ \frac{\lambda+\mu}{4\rho}\frac{\Delta t^2}{\Delta x\Delta z}\left(u_z^{\,i+1,j,k+1,l} - u_z^{\,i+1,j,k-1,l} - u_z^{\,i-1,j,k+1,l} + u_z^{\,i-1,j,k-1,l}\right)
\end{aligned}
$$

$$
\begin{aligned}
u_y^{\,i,j,k,l+1} &= 2u_y^{\,i,j,k,l} - u_y^{\,i,j,k,l-1} + \frac{\lambda+2\mu}{\rho}\frac{\Delta t^2}{\Delta y^2}\left(u_y^{\,i,j+1,k,l} - u_y^{\,i,j,k,l} + u_y^{\,i,j-1,k,l}\right) \\
&+ \frac{\mu}{\rho}\frac{\Delta t^2}{\Delta x^2}\left(u_y^{\,i+1,j,k,l} - u_y^{\,i,j,k,l} + u_y^{\,i-1,j,k,l}\right) + \frac{\mu}{\rho}\frac{\Delta t^2}{\Delta z^2}\left(u_y^{\,i,j,k+1,l} - u_y^{\,i,j,k,l} + u_y^{\,i,j,k-1,l}\right) \\
&+ \frac{\lambda+\mu}{4\rho}\frac{\Delta t^2}{\Delta x\Delta y}\left(u_x^{\,i+1,j+1,k,l} - u_x^{\,i+1,j-1,k,l} - u_x^{\,i-1,j+1,k,l} + u_x^{\,i-1,j-1,k,l}\right) \\
&+ \frac{\lambda+\mu}{4\rho}\frac{\Delta t^2}{\Delta y\Delta z}\left(u_z^{\,i,j+1,k+1,l} - u_z^{\,i,j+1,k-1,l} - u_z^{\,i,j-1,k+1,l} + u_z^{\,i,j-1,k-1,l}\right)
\end{aligned}
$$

$$(3\text{-}4)$$

$$u_z^{i,j,k,l+1} = 2u_z^{i,j,k,l} - u_z^{i,j,k,l-1} + \frac{\lambda+2\mu}{\rho}\frac{\Delta t^2}{\Delta z^2}\left(u_z^{i,j,k+1,l} - u_z^{i,j,k,l} + u_z^{i,j,k-1,l}\right)$$

$$+ \frac{\mu}{\rho}\frac{\Delta t^2}{\Delta x^2}\left(u_z^{i+1,j,k,l} - u_z^{i,j,k,l} + u_z^{i-1,j,k,l}\right) + \frac{\mu}{\rho}\frac{\Delta t^2}{\Delta y^2}\left(u_z^{i,j+1,k,l} - u_z^{i,j,k,l} + u_z^{i,j-1,k,l}\right)$$

$$+ \frac{\lambda+\mu}{4\rho}\frac{\Delta t^2}{\Delta x \Delta z}\left(u_x^{i+1,j,k+1,l} - u_x^{i+1,j,k-1,l} - u_x^{i-1,j,k+1,l} + u_x^{i-1,j,k-1,l}\right)$$

$$+ \frac{\lambda+\mu}{4\rho}\frac{\Delta t^2}{\Delta y \Delta z}\left(u_y^{i,j+1,k+1,l} - u_y^{i,j+1,k-1,l} - u_y^{i,j-1,k+1,l} + u_y^{i,j-1,k-1,l}\right),$$

where superscripts i, j, k, and l, denote the grid number in x, y, z, and t direction, respectively. Δx, Δy, and Δz are the spatial grid spacing, being taken as the same value of $\Delta h = 1.0$ km, and Δt is the time increment of the FDM calculation, being taken as 0.05 s to satisfy the stability condition for 3-D wave propagation [Aki and Richards, 1980],

$$\Delta t / \Delta h \le \left(V_P^2 + V_S^2\right)^{-1/2}. \tag{3-5}$$

The calculation with half grid spacing and time increment results was also performed and resulted in the similar result. The crustal structure is the same as the one used in the Green's function calculation (Table 2-2) . Then, if every boundary condition is given by displacements, equations (3-4) are solved for each time step.

Assuming symmetry across the fault plane ($y = 0$), the displacements in two directions, u_x and u_z, on the fault plane are given as half of the slip of the kinematic model. The fault-normal displacement u_y is calculated by the continuities of fault-normal traction τ_{yy}. In this case, the symmetry reduces this condition as,

$$\tau_{yy} = 0, \tag{3-6}$$

which is represented in the FDM manner:

40

$$\lambda \frac{u_x^{i+1,0,k,l} - u_x^{i-1,0,k,l}}{2\Delta x} + (\lambda + 2\mu)\frac{u_y^{i,1,k,l} - u_y^{i,0,k,l}}{\Delta y} + \lambda \frac{u_z^{i,0,k+1,l} - u_z^{i,0,k-1,l}}{2\Delta z} = 0 . \tag{3-7}$$

This equation determines the value of u_y on the fault plane $u_y^{i,0,k,l}$, because the all other displacements in (3-7) have been given as boundary conditions or calculated by equation (3-4).   The continuities of τ_{xy} and τ_{yz} are easily confirmed from equation (3-2) using the fact that u_x and u_z are odd functions and u_y is even function.

The boundary condition on the free surface is traction free condition, *i.e.*,

$$\tau_{xz} = \tau_{yz} = \tau_{zz} = 0 \quad \text{at} \quad z = 0 \tag{3-8}$$

A possible way to solve (3-8) numerically is to introduce the concept of fictitious displacements [Alterman and Karal, 1968; Mikumo *et al.*, 1987] at the free surface.   The fictitious displacement just above the free surface $u_x^{i,j,-1,l}$, $u_y^{i,j,-1,l}$, and $u_z^{i,j,-1,l}$ may be calculated as follows from equation (3-8) by extending artificial grid points at a distance Δz above the surface:

$$u_x^{i,j,-1,l} = u_x^{i,j,1,l} + \frac{\Delta z}{\Delta x}\left(u_z^{i+1,j,k,l} - u_z^{i-1,j,k,l}\right)$$

$$u_y^{i,j,-1,l} = u_y^{i,j,1,l} + \frac{\Delta z}{\Delta y}\left(u_z^{i,j+1,k,l} - u_z^{i,j-1,k,l}\right)$$

$$u_z^{i,j,-1,l} = u_z^{i,j,1,l} + \frac{\Delta z}{\Delta x}\frac{\lambda}{\lambda+2\mu}\left(u_x^{i+1,j,k,l} - u_x^{i-1,j,k,l}\right) + \frac{\Delta z}{\Delta y}\frac{\lambda}{\lambda+2\mu}\left(u_y^{i,j+1,k,l} - u_y^{i,j-1,k,l}\right). \tag{3-9}$$

By using the above expressions, $u_x^{i,j,-1,l}$, $u_y^{i,j,-1,l}$, and $u_z^{i,j,-1,l}$ are calculated for each time step, and then applied as a boundary condition in the calculation of the next time step.   Without boundary conditions on the other four boundaries, the calculation is carried out until the reflected waves from these boundaries arrive at the assumed fault plane.

Once every displacement in the elastic medium is determined, the stress components other than τ_{yy}

are determined by equations (3-2), which are written in the finite difference manner as followings:

$$\tau_{xx}^{\,i,0,k,l} = \frac{\lambda+2\mu}{2\Delta x}\left(u_x^{\,i+1,0,k,l} - u_x^{\,i-1,0,k,l}\right) + \frac{\lambda}{\Delta y}\left(u_y^{\,i,1,k,l} - u_y^{\,i,0,k,l}\right) + \frac{\lambda}{2\Delta z}\left(u_z^{\,i,0,k+1,l} - u_z^{\,i,0,k-1,l}\right)$$

$$\tau_{zz}^{\,i,0,k,l} = \frac{\lambda}{2\Delta x}\left(u_x^{\,i+1,0,k,l} - u_x^{\,i-1,0,k,l}\right) + \frac{\lambda}{\Delta y}\left(u_y^{\,i,1,k,l} - u_y^{\,i,0,k,l}\right) + \frac{\lambda+2\mu}{2\Delta z}\left(u_z^{\,i,0,k+1,l} - u_z^{\,i,0,k-1,l}\right)$$

$$\tau_{xy}^{\,i,0,k,l} = \frac{\mu}{2\Delta x}\left(u_y^{\,i+1,0,k,l} - u_y^{\,i-1,0,k,l}\right) + \frac{\mu}{\Delta y}\left(u_x^{\,i,1,k,l} - u_x^{\,i,0,k,l}\right)$$

$$\tau_{yz}^{\,i,0,k,l} = \frac{\mu}{2\Delta z}\left(u_y^{\,i,0,k+1,l} - u_y^{\,i,0,k-1,l}\right) + \frac{\mu}{\Delta y}\left(u_z^{\,i,1,k,l} - u_z^{\,i,0,k,l}\right)$$

$$\tau_{xz}^{\,i,0,k,l} = \frac{\mu}{2\Delta x}\left(u_z^{\,i+1,0,k,l} - u_z^{\,i-1,0,k,l}\right) + \frac{\mu}{2\Delta z}\left(u_x^{\,i,0,k+1,l} - u_x^{\,i,0,k-1,l}\right). \tag{3-10}$$

3-2   Determination of Stress Distribution

Fig. 3-2 shows the history of the FDM calculation described in the previous section: three components of the slip vector and six components of the stress tensor everywhere on the fault plane at each 1 s time interval.   Among them, u_x, u_z ,and τ_{yy} is given as boundary conditions and the other six components are determined through calculation.   Fault-normal displacement u_y has non-zero value, not indicating separation of fault surfaces but the movement of closed fault plane.   The shear stress τ_{xy} and τ_{yz} represent similar distributions to the corresponding strike displacement u_x and u_z. Since most of the rupture of this earthquake is right-lateral strike-slip and has larger u_x than other components, hereafter we focus on the relations between shear stress τ_{xy} and slip u_x.

The maximum stress drop in τ_{xy} is about 5 MPa near the hypocenter, not at the region of maximum slip.   A small stress increase of less than 2 MPa appears outside of the ruptured area,

much smaller than infinite stress increases having a square root singularity theoretically calculated for the crack with conventional friction law of static and dynamic friction levels [*e.g.*, Madariaga, 1976]. This may be because of the insufficient resolution due to the basis function expansion, the smoothing constraint in the inversion, and frequency band-limited data, which smeared out the fine structures of the stress buildup process.   To estimate the maximum stress before the rupture, namely strength at each point, finer knot spacing and more precise knowledge about crustal structure are necessary.

3-3   Constitutive Relations

The calculated distribution of slip and stress can be used to give the constitutive relation at each grid point in space.   Fig. 3-3 shows the relations plotted at each time step up to 30 s after rupture initiation for the points where the slip-rate functions are shown in Fig. 2-7.   At almost every point, stress decreases with increasing slip (slip-weakening) as seen in frictional experiment of rocks (Fig. 1-3b).   Evidently, the slip-weakening rate ($du_x/d\tau_{xy}$) in the shallow parts (**a-d**) are smaller than those in the deeper parts (**e-j**).   This difference corresponds to the differences of the durations of slip-rate functions, or rise time, as discussed in the next chapter: longer rise time with small slip-weakening rate and short rise time with large slip-weakening rate.   From the view point of the slip-weakening critical displacement D_c, the one in the shallow part of the crust is about 1 m and tends to be larger than the one deeper in the crust, about 50 cm.   One possible factor that may explain such difference is the assumed horizontally layered structure (Table 2-1) in which the rigidity of the shallowest layer (0 - 3 km) is lower than those of deeper layers.   However, the difference in slip-weakening rate is too large to be explained by low rigidity.   The behavior of stress after slip termination is also different due because of the free surface.   At the shallow points stress continues to decrease after slip termination, since the reflected waves by the free surface reduce stress further.   In contrast, at the deeper points the effects of reflected waves are negligible and stress is built-up by successive

43

stress decreases at the neighbor points.

The relation between slip rate and stress is sometimes used as a constitutive law in simulation of earthquakes [Carlson and Langer, 1989; Cochard and Madariaga, 1994].   Heaton [1990] suggested that the velocity-weakening constitutive relation in the slip decelerating process is important to explain slip-pulse-like propagation of rupture that is common in many earthquakes.   This is demonstrated by the simulation of dynamic rupture in a 2-D plane with velocity-weakening constitutive relations [Cochard and Madariaga, 1994] or modified rate- and state-dependent constitutive relations [Beeler and Tullis, 1996].   Fig. 3-4 shows the relations between slip rate and stress shown in the same manner as the slip-stress relations.   Although the velocity-weakening in the slip accelerating process is visible, this is trivial and easily predicted by slip-weakening relations.   On the other hand, velocity-weakening behavior is unclear in the slip decelerating process.   However, it is difficult to determine by waveform inversion because rupture at small rate may be hidden by noise. This result alone cannot prove that stress is independent of slip-rate.

3-4   Resolution Analysis

Since the analysis in the present study adopts expansion by basis functions, band-pass filtering of the data and Green's functions, and smoothing constraints in the inversion, the results are affected by these smoothing factors.   The simulation procedure is illustrated by Fig. 3-5.   First, a dynamic rupture of a 3-D crack is calculated by the method of Mikumo *et al.* [1987], with a classical friction law of static and dynamic friction.   The shape of the crack area is assumed to be similar to the ruptured area of the Kobe earthquake, and the rupture velocity and the stress drop are 2.5 km/s and 5 MPa, everywhere in the crack area.   Fig. 3-6a shows the spatial distribution of slip and slip-rate functions at selected five points on the crack plane calculated for the original crack model.

44

Although slip-rate functions show high-frequency vibrations because of discretization in the FDM, they are reduced by the following band-pass filtering and do not affect the results.

Seismic waves, which is called target synthetic seismograms, from this source are calculated using Green's functions used in the actual inversion, and band-pass filtered between the frequency range from 0.025 to 0.5 Hz, the same as the actual analysis. These target seismograms are then inverted as data, and the spatial distributions of slip and slip-rate functions are obtained (Fig. 3-6b). The basis functions are the same as the previous inversion, and the proper weights of smoothing constraints are estimated by ABIC. High gradients at the crack tip of the target spatial distribution and at the initial parts of the slip-rate functions cannot be reproduced, whereas the overall distribution and the rise times resemble those of the target. No clear depth dependency appears in the rise times.

FDM calculation followed using this kinematic model to obtain the constitutive relations. Fig. 3-7 represents the constitutive relations introduced in the crack model and the calculated ones at five points on the crack surface. Although the original constitutive relation should show prompt reduction of stress as slip reaches zero, the FDM calculation produces artificial slip-weakening relations due to finiteness of the time increment and spatial spacing. The calculated constitutive relations have a smaller slip-weakening rate than this artificial rate. This is mainly due to the band-limited data, up to 0.5 Hz, and the smoothing constraints, and the effect of expansion by basis function is smaller because it is sufficiently fine in this frequency range. Unlike as the actual data analysis (Fig. 3-3), these relations show little depth dependency and the slip-weakening rates are almost the same at every depth. The slip-weakening rate is about 5 MPa/m which represents the resolution limit inherent in this analysis, and is similar to those in the deeper part of the previous results (Fig. 3-3, **e-j**). Therefore, in the previous result the constitutive relations on the deeper part of the fault are obtained under this resolution limit, hence it is quite questionable whether this relation is realistic. The estimated values of D_c of about 50 cm from these relations has no significance other

45

than an upper limit of D_c in the actual rupture process.   On the other hand, the slip-weakening rate in the shallow crust is smaller than this limit and it is plausible that it is well determined by this method. The slip-weakening rate may be small or the critical displacement D_c is large in the shallow crust.
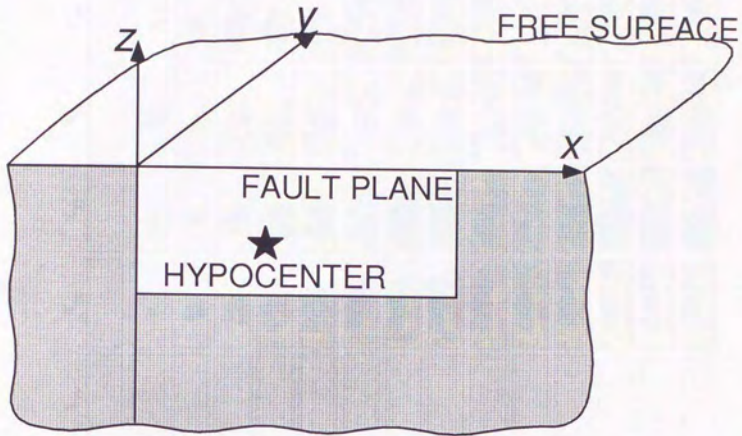
Fig. 3-1 Geometry of three-dimensional space used in the present finite difference calculations.
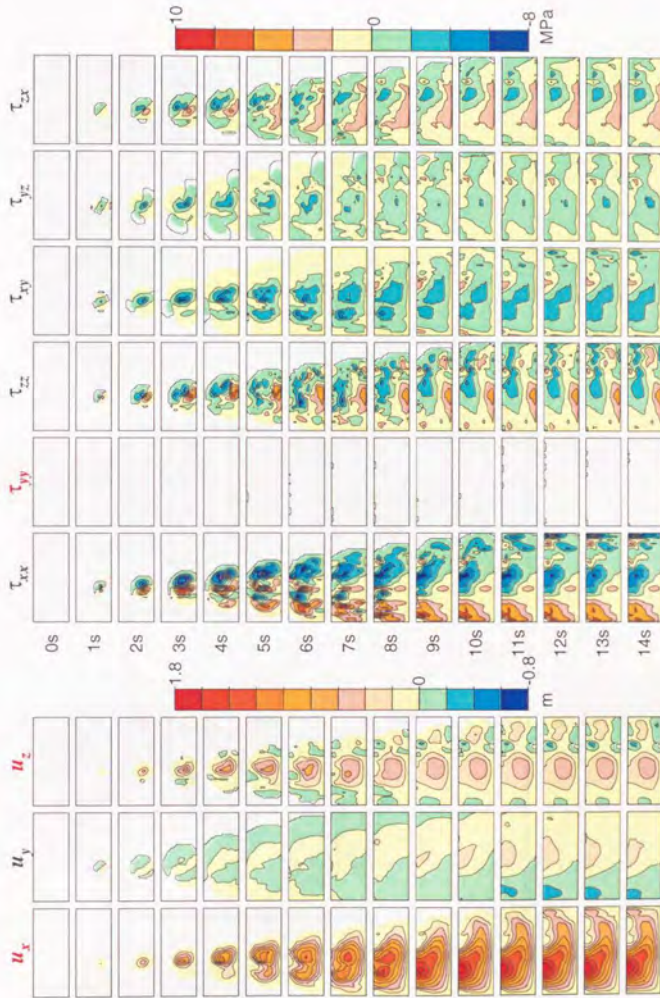
Fig. 3-2 The histories of each component of the slip vector and the stress tensor. u_x and u_z represent the kinematic results and are given as boundary conditions, τ_{yy} is fixed to be zero.

48
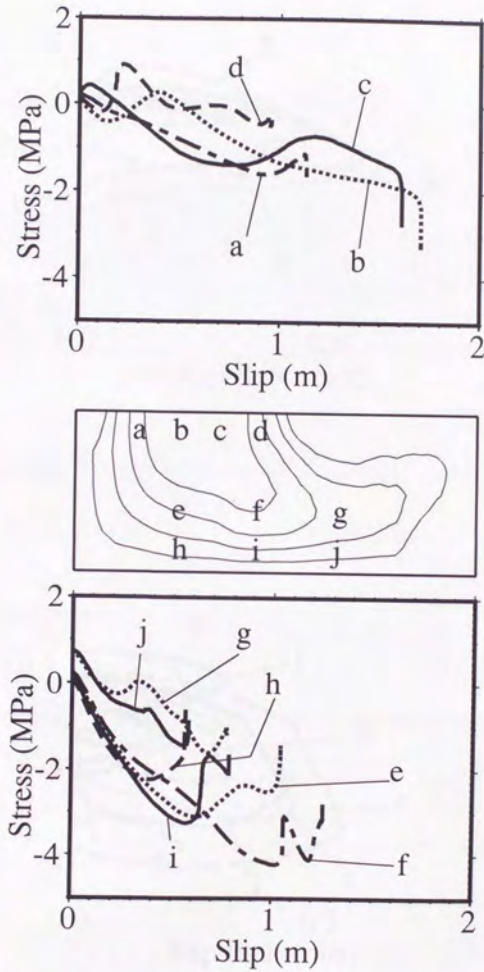
Fig. 3-3 The constitutive relation between slip and stress on the fault plane. Each trace is the
function calculated at the corresponding location shown in the middle figure of slip distribution.
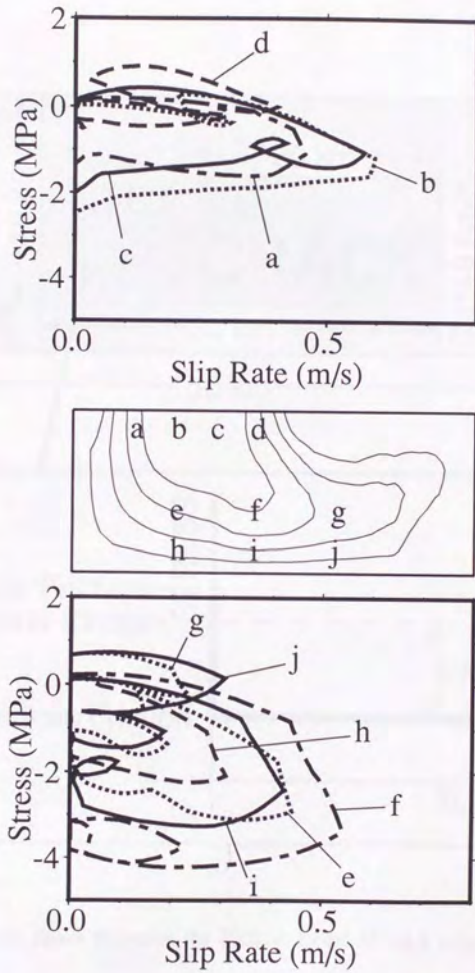
Fig. 3-4 Same as Fig. 3-3 although the relation between slip rate and stress on the fault plane is shown.
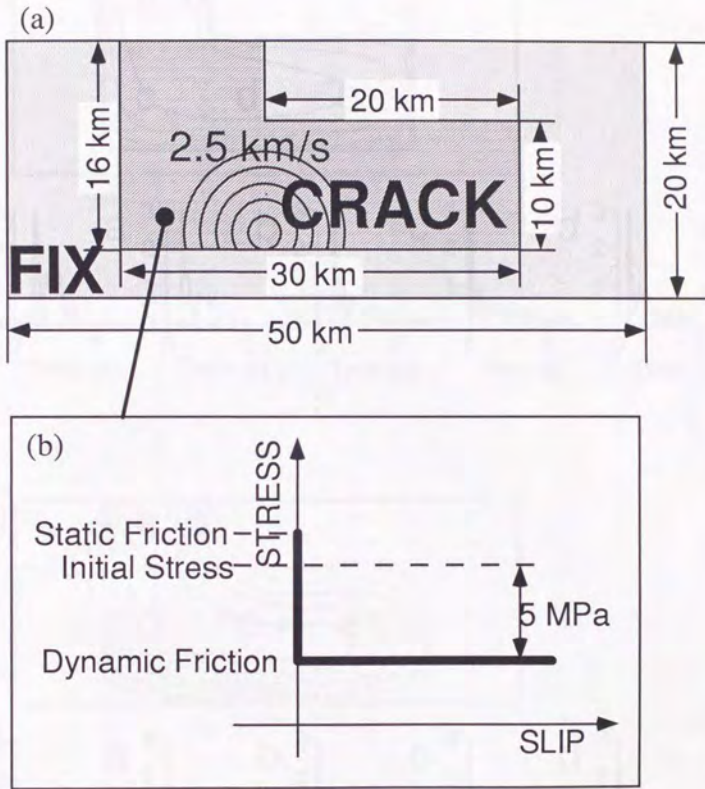
Fig. 3-5 (a) Schematic figure illustrates the dynamic model of crack propagation with a classical friction law shown in (b) as a constitutive relation.   This model is used as the target model.
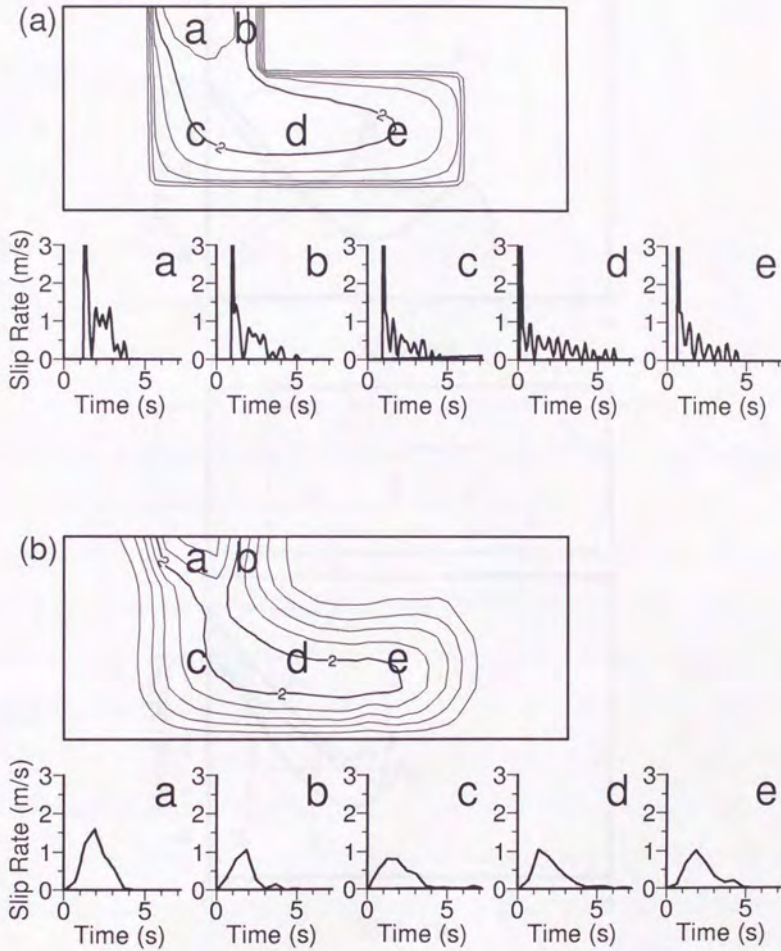
Fig. 3-6 Slip distributions and slip-rate functions (a) calculated by dynamic crack model and (b)

obtained by inversion using the target seismograms.
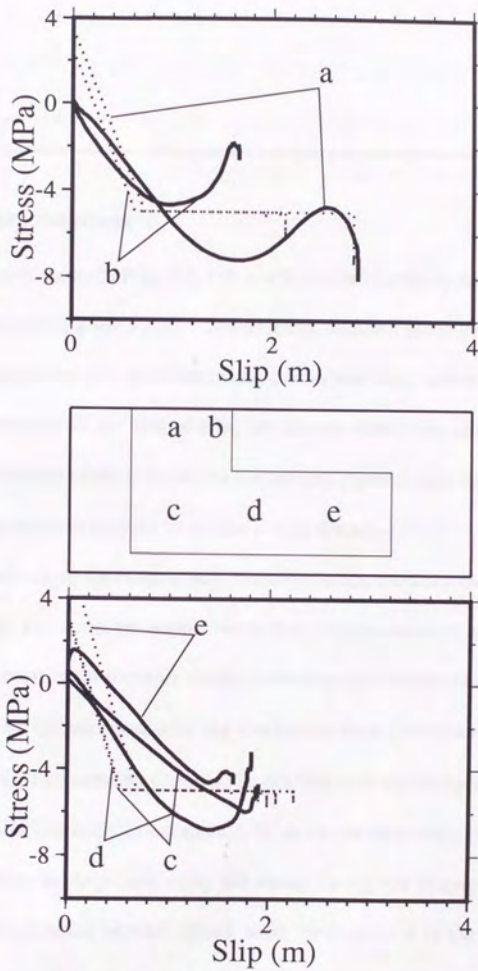
Fig. 3-7 The constitutive relation between slip and stress on the fault plane as the result of the simulation.   Each trace is the function calculated at the corresponding location shown in the middle figure of slip distribution.

Chapter 4

Discussion

4-1   Alternative Solutions

The slip distribution shown in Figs. 2-6, 2-7, and 2-8 is the objectively determined unique solution based on a Bayesian modeling and ABIC.   Nevertheless, different distributions can be obtained from different model assumptions, *i.e.*, prior information, basis functions, crustal structure, and the data. Among possible variation of the assumptions, we discuss about two cases that produces useful implication to the reliability of the solution: the one assuming geometrical barrier near the hypocenter and the other using short knot interval for temporal basis function.

The surface offsets along the Nojima fault diminished at the northern end of Awaji Island, and in Akashi strait and in the northeast region no surface rupture directed northeast-southwest was discovered.   While most of the previous studies introduced the discontinuities of fault plane beneath Akashi straits to obtain discontinuous total slip distribution there [Yoshida *et al.*, 1996; Sekiguchi *et al.*, 1996; Wald 1996], I assumed no discontinuity but that total slip changes smoothly across whole fault plane using spatial constraint in equation (2-7), as my previous study [Ide *et al.*, 1996a].   The obtained rupture history in the present study still shows the rupture propagation in the two distinct directions from the hypocenter beneath Akashi strait, *i.e.*, region **A** to the northeast and **B** to the southwest in Fig. 2-8, inferring some geometrical discontinuities.   If these discontinuities prevent slip on it, the assumption of smoothing constraint across whole assumed fault plane may be improper and another constraint taking these discontinuities into account should be used.

In this section, I adopt such smoothing assumption represented by another spatial constraint

matrix D_1, being the same as in equation (2-7) with the exception that it constrains the slip to be zero on a vertical line, practically 2.5 km southwest of the hypocenter.   The inversion yields a solution having slip discontinuity beneath Akashi strait (Fig. 4-1).   At first look, this distribution seems different from the previous result (Fig. 2-6).   However the difference is limited in the region near the subjected non-slip line, and two distributions are quite similar in the other part of the fault plane. The agreement between observed and calculated displacement is nearly the same as the previous result, hence it is impossible to conclude whether such a slip discontinuity exists or not, from the seismic wave analysis alone.

The stress distribution is determined by the FDM with the boundary condition of this slip distribution, and hence constitutive relations are obtained for this smoothing assumption (Fig. 4-2), in which the differences from the previous constitutive relations (Fig. 3-3) are limited in the region near the subjected non-slip line (at point C), and similar relations are obtained at other points.   Although the slip discontinuities alter appearance of the slip distribution, the characteristic of the slip-weakening behavior and the depth dependencies of slip-weakening rate are unchanged.   Therefore, it is not necessary for the discussion about overall constitutive relations whether the slip discontinuities exist beneath Akashi strait.

The other model setting adopts the short knot interval of temporal basis functions.   One of the characteristics of the spatio-temporal slip distribution is the long rise times of about 5 s in the shallow region of the fault plane (Fig. 2-7).   One may questioned whether this is an artifact due to the smoothing constraints and the long knot interval and long time window (7.2 s) in which each slip-rate function is determined.   In this case, the observed waves can also be explained by the model with short knot interval and short time window.   To answer this question, two other inversions are performed, employing two short knot intervals of temporal basis function, 0.4 s and 0.3 s, and maintaining the number of basis functions.   The proper weights of the smoothing constraints are

estimated by ABIC.

Fig. 4-3 shows the slip-rate functions for these model settings with those of the original model. The interval of 0.4 s corresponds to the time window of 4.8 s, which is comparable to the longest rise time. In this case, as a matter of course, the ABIC gives the similar smoothness of slip-rate functions as the original, independent of knots interval, and the slip-rate functions are almost the same as the original ones. Although its synthetic waves agree with the observed data as well as the original ones, there are unnatural truncations of slip-rate functions at some shallow points (*e.g.*, C in Fig. 4-3), being improper to be used as boundary conditions of FDM calculation. Such truncation results in an artificial sharp corner in constitutive relation.

On the other hand, 0.3 s interval forms 3.6 s time window. This yields similar slip-rate functions at deeper points of fault plane, whereas those at shallow points are quite different from the other two cases. This short time window does not only truncate the original functions, but alter their shapes significantly at shallow points. As a result, the agreement between the observed and calculated displacement is worse than those of the other two cases. It is obvious that this result with 0.3 s interval is not proper for the following stress calculation.

This analysis indicates that the long rise times of about 5 s determined in the previous chapters are not intrinsic result due to the long knot interval and long time window, and that the interval of 0.6 is appropriate to express slip-rate functions without truncation. A long rise time of 5 s should be obtained by the analysis in the frequency range of this study, lower than 0.5 Hz, and the time window of 3.6 s is too short. However, it should be noted that this long rise time includes the effect of the propagation of rupture because of the lack of the resolution.

4-2   Constitutive Relations in Shallow Crust

As shown in the previous chapter, the constitutive relations in the shallow parts are different from those in the deeper parts, which must be associated with some characteristic phenomena in the shallower part of the crust.   A well-known such phenomenon is paucity of very shallow seismicity. The aftershock seismicity of the Kobe earthquake in the shallowest (0 - 3 km) region was quite low along the Nojima fault (Fig. 2-1b), where the total slip amount is the largest.   It is generally known that seismicity is usually low in the shallow part of faults with well-developed gouge, *e.g.*, Marone and Scholz [1988] indicated for several fault systems of different periods in western United State (Fig. 4-4).

Some mechanisms are proposed to explain the shallow paucity of seismicity.   Based on laboratory experimental friction studies indicating that thick layers of simulated gouge exhibit a positive slip-rate dependence of frictional resistance (velocity strengthening) at slow slip velocities of about 0.01 - 10 µ/s order [*e.g.*, Marone *et al.*, 1990], Marone and Scholz [1988] attributed the paucity of shallow seismicity to velocity strengthening behavior of unconsolidated materials between fault planes.   Velocity strengthening behavior may stabilize fault slip and prevent earthquake instability, and moreover this mechanism may play key roles for afterslip occurrence and creep phenomena as pointed out by Marone *et al.* [1991].

On the other hand, Scholz [1988] suggested that a large critical distance D_c stabilizes slip in the shallow region of the fault.   He related D_c to the minimum size of the contact junctions of geometrically unmated fractal surfaces under a normal stress, and showed only large scale junctions are built by relatively low normal stress in the shallow region.   Therefore, D_c becomes large enough to prevent the seismic nucleation process in the shallow crust.   Marone and Kilgore [1993] presented another interpretation of large D_c based on laboratory experiment, in which D_c is controlled by the thickness of gouge zones that may be thick in the shallow region.

In the present study, no velocity-strength constitutive relation appears, while D_c is larger (about 1 m) in the shallow region.   This supports the possibility of large D_c as a mechanism related to the paucity of shallow seismicity rather than the velocity-strengthening behavior.   My model supplies no information about the physical interpretation of large D_c, and there are other mechanisms accountable for paucity of shallow; combined brittle-creep process is suggested by Ben-Zion [1996] and the effects of fluid must be considered.   Whether D_c is generally responsible for seismicity should be studied for many other fault systems.

4-3   Rise Time in the Other Earthquakes

The analysis of the Kobe earthquake shows that small slip-weakening rate in the shallow crust corresponds to a long rise time.   It is proved that small slip-weakening rate is generally associated with a long rise time by simple simulations of 2-D antiplane shear crack similar to the analysis of the previous chapter.   In this simulation, spatio-temporal slip distribution on a 2-D antiplane crack is given as boundary conditions by a slip-rate function having rise time T_r and the starting time of each function at every point of the crack, which is determined by a constant rupture propagation velocity. The geometry of the spatio-temporal distribution of slip rate is illustrated in Fig. 4-5a.   The shapes of all the slip-rate functions are the same and assumed as a similar one to that calculated with a classical friction law (Fig. 4-5b).   For three different rise times T_r stress history and constitutive relation are calculated.   Since the slip amounts are identical among these three cases, longer duration means small slip-rate that is roughly in proportional with dynamic stress drop.   As a result, longer slip duration yields smaller stress decrease rate in constitutive relations (Fig. 4-6).   This indicates that the depth dependency of constitutive relation can be roughly estimated by the depth dependency of rise time determined by waveform inversion for other earthquakes.

The earthquake that has large surface offset and was analyzed in detail by near-field strong-motion records is quite rare and the only example other than the Kobe earthquake is the 1992 Landers, California, earthquake [Wald and Heaton, 1994; Cohee and Beroza, 1994; Cotton and Campillo, 1995]. For this earthquake, the rise time in the shallow crust is reported to be longer than in the deeper parts [Wald and Heaton, 1994], hence it is probable that the Landers earthquake was characterized by the same dependency of the stress decrease rate as in the Kobe earthquake. However, as Cotton and Campillo [1995] questioned this long rise time in the shallow crust because of the lack of resolution, more study is necessary to assure this conclusion.

The 1979 Imperial Valley earthquake is the similar to the Kobe earthquake and the Landers earthquake in that it is a strike-slip event in the shallow crust. Unlike the Kobe and the Landers earthquakes, this earthquake has small slip in the shallow part of the assumed fault plane, and the depth dependency of the rise time is not clear [Archuleta, 1984]. Instead of long rise time, the negative stress drop, namely stress increase, during slip at shallow crust is suggested for this earthquake. Quin [1990] constructed a dynamic crack model with a classical friction law with static and dynamic friction levels based on the kinematic model of Archuleta [1984] and showed that a negative stress drop is necessary to reproduce the slip distribution of the kinematic model (Fig. 4-7). Since a classical friction law is assumed in the model, it should be discussed if this negative stress drop is necessary even in slip-weakening model like my studies. However, the difference between positive stress-drop in the deeper crust and negative stress drop in the shallower crust implies some difference in constitutive relations for the Imperial Valley earthquake. Although these samples are quite few, the difference of constitutive relations at depth may be found in other earthquakes that produced surface fault offsets.

☆ Hypocenter   ⟶ Slip (1m)
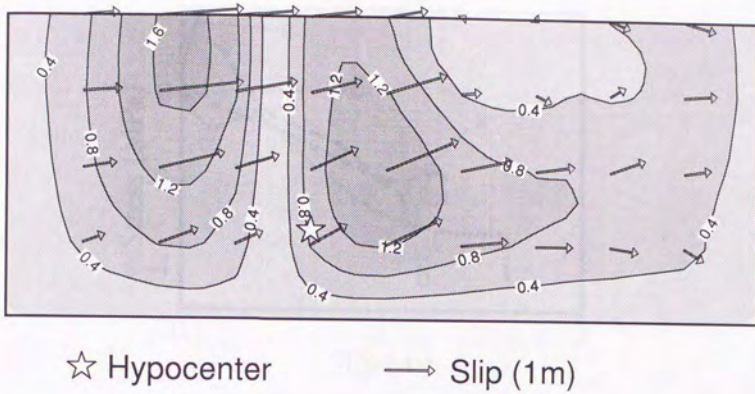
Fig. 4-1 The distribution of total slip and slip vector on the fault plane for the model including slip discontinuity beneath Akashi strait.   Each vector represents the slip magnitude and angle at the point.
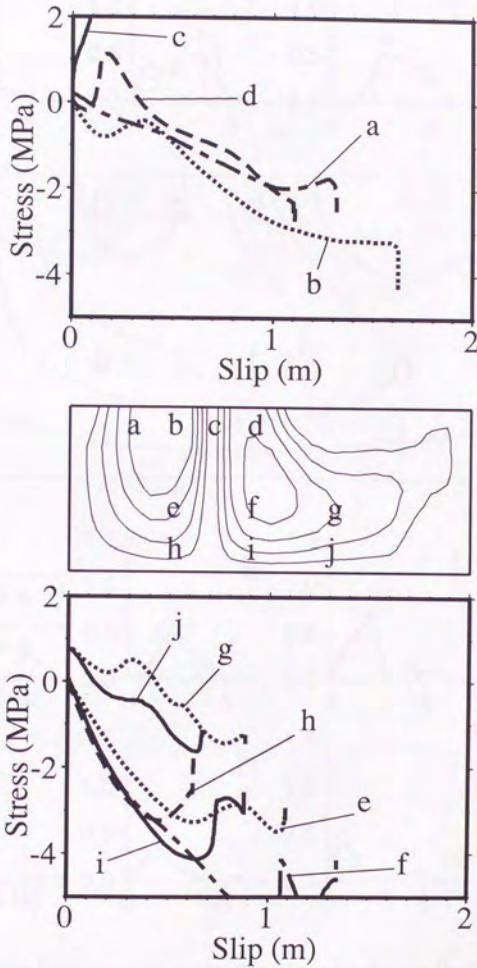
Fig. 4-2 The constitutive relation between slip and stress on the fault plane for the model including slip discontinuity beneath Akashi strait.   Each trace is the function calculated at the corresponding location shown in the middle figure of slip distribution.

61
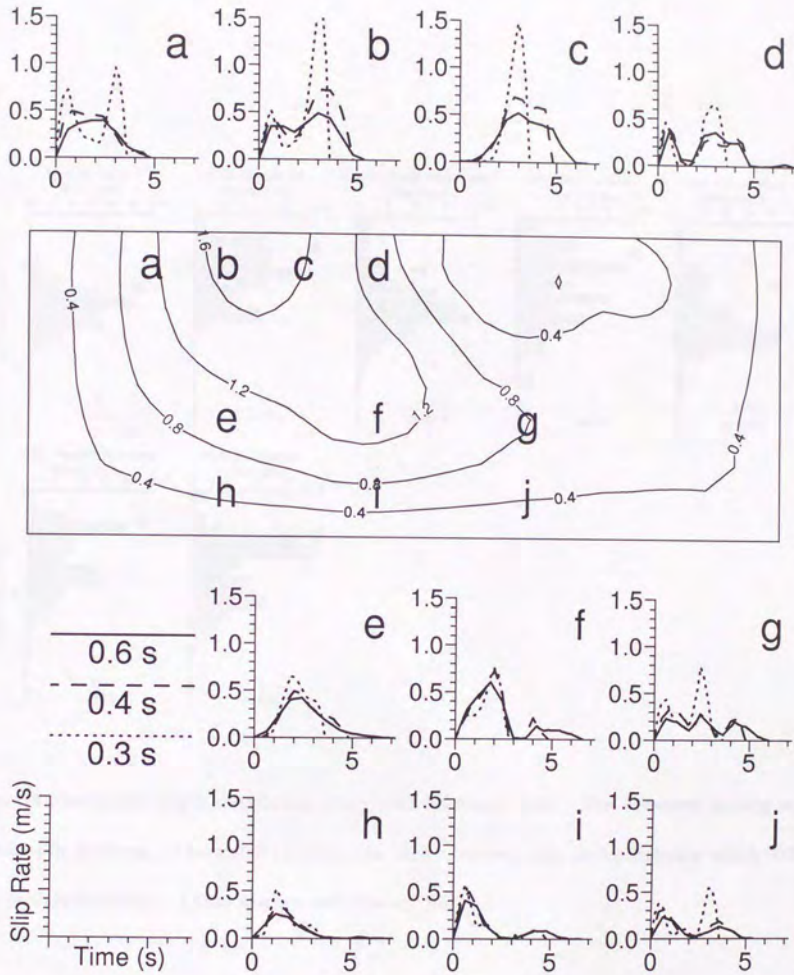
Fig. 4-3 The slip-rate functions at ten points shown by **a-j** in the slip distribution.   The solid, dashed and dotted lines show change of slip rate within 7.2 s after the arrival of imaginary rupture determined with the knot intervals of 0.6 s, 0.4 s, and 0.3 s, respectively.
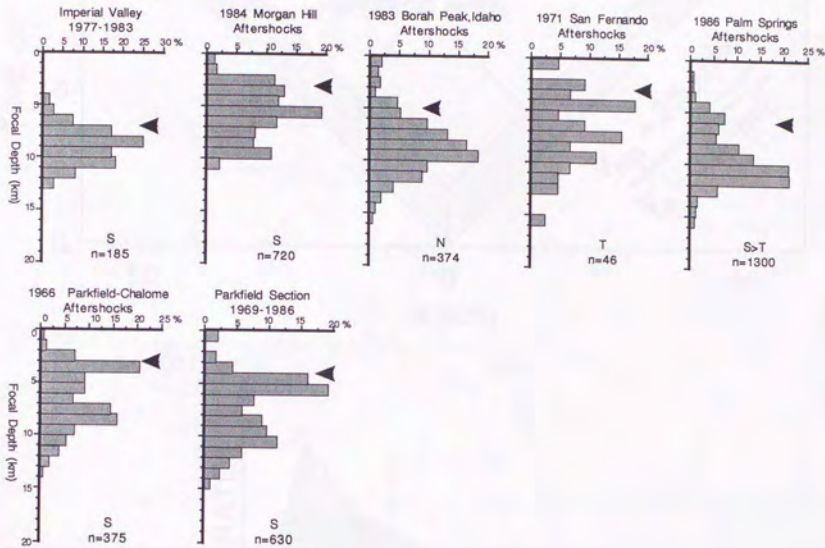
Fig. 4-4 Earthquake depth distribution along well-developed fault.   The dominant faulting mode (strike-slip, S; thrust, T; normal, N) is shown for each.   Arrows indicate depths below which 90% of the earthquake occur.   (After Marone and Scholz [1988].)
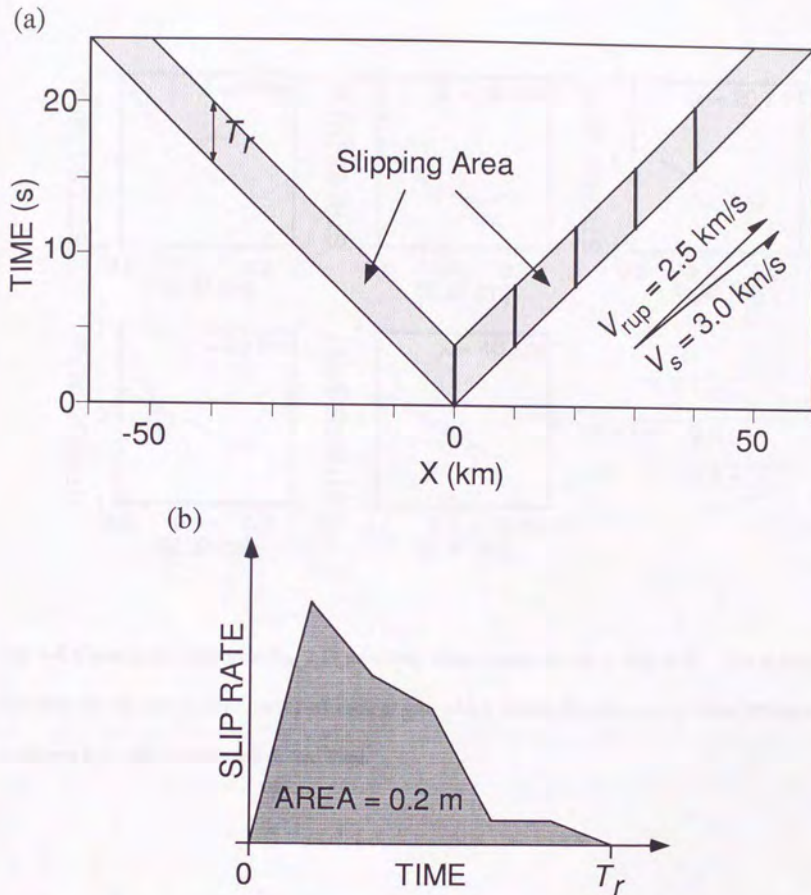
Fig. 4-5 (a) Schematic diagram of 2-D antiplane shear crack propagation.   (b) The slip-rate history at each point on the crack surface.   The shaded area is slipping with this history and slip-stress relation is evaluated on the bold lines, x = 0, 10, 20, 30, and 40km.   Calculation is carried out with different values of T_r, maintaining the area of the slip-rate function, namely slip amount.
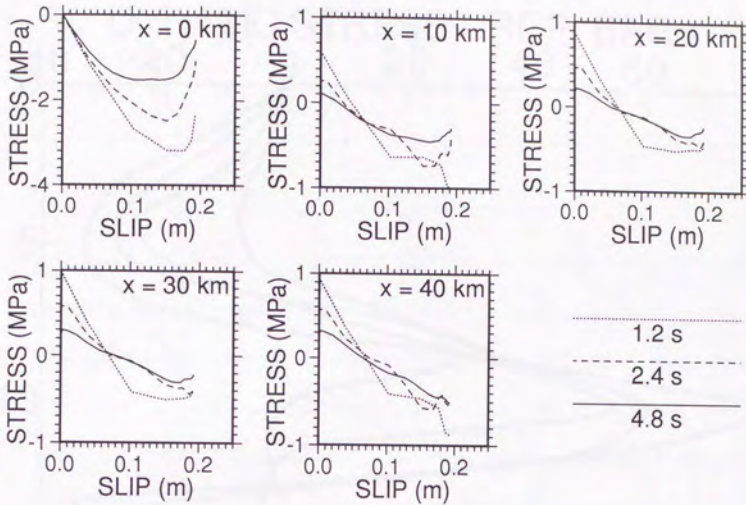
Fig. 4-6 Constitutive relations for 2-D antiplane shear crack shown in Fig. 4-2.   The location is specified on the upper-right corner of each graph, which shows the relations of three different slip durations by solid, dashed, and dotted lines.
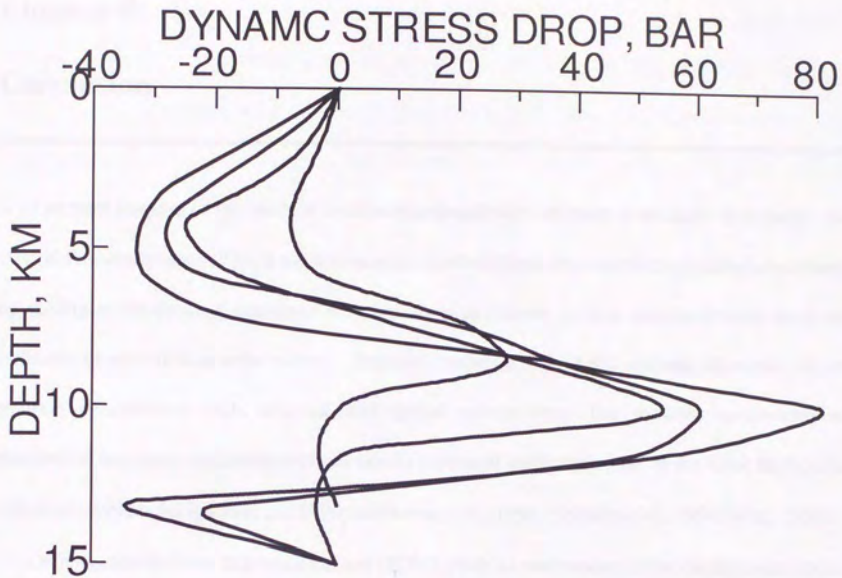
Fig. 4-7 Cross section of dynamic stress drop with depth along four profiles of the dynamic source model of the 1979 Imperial Valley, California, earthquake.   (After Quin [1990].)

Chapter 5

Conclusion

The main purpose of this study is to determine constitutive relations of an actual earthquake, the 1995 Kobe earthquake. This is the first attempt in which shear stress on the fault plane is calculated by solving elasto-dynamic equations with boundary conditions of fault slip distribution based on inversion of near-field seismic waves. Bayesian modeling with ABIC ensures objectivity of the solution of inversion with temporal and spatial constraints. The resultant spatio-temporal distribution has many similarities with previously presented kinematic model of the Kobe earthquake [Ide *et al.*, 1996a; Sekiguchi *et al.*, 1996; Horikawa *et al.*, 1996; Yoshida *et al.*, 1996; Wald, 1996].

Computation by finite difference method (FDM) yields all components of the displacement vector and the stress tensor everywhere in the elastic medium surrounding the fault plane, and on the fault plane, too. Constitutive relations are then obtained as the relation between the shear stress and slip in strike direction on the fault plane, by connecting them at each time step of FDM calculation. At almost all points having large slip, the relations show slip-weakening behavior, whose rates depend on the depth and are smaller in the shallow region than those deeper. A simulation with a crack model to verify the resolution of my method concludes that the resolution is not high enough in the deep region of the fault plane. The obtained slip-weakening rates should be regarded as lower limits and D_c of 50 cm should be regarded as upper limits at deep region. At shallow region, the slip-weakening rate is more than resolution limit and characteristic distance D_c is estimated to be about 1 m or more.

Many researchers predicted such differences of constitutive relations and attributed to them the reason of paucity of shallow seismicity generally observed on mature fault system.   The first study to infer the difference is the dynamic study of the 1979 Imperial Valley earthquake by Quin [1990], in which constitutive relation is not obtained but assumed to be a classical friction law with static and dynamic friction levels.   The result showed the stress in the shallow region must be raised during fault slippage, namely negative stress drop, where usually stress drops positively.   My conclusion also indicates the anomaly of shallow fault slip but in the different manner: the slip-weakening rate is small in the shallow part.   Existence of unconsolidated material along the fault and the low normal stress in the shallow crust strongly suggests that the constitutive relations are different, and my result and the other evidence in the kinematic model and dynamic model support this.   However, further studies on many other actual earthquakes are necessary to conclude how it differs.

The most serious problem in the study of an actual earthquake using observed seismic waves is that the resolution is insufficient to reveal fine structures of the earthquake source.   The lack of knowledge about crustal structure is significant in this problem.   However, even when accurate crustal structure is known and Green's functions are calculated precisely for every source to receiver combination, another difficulty arises from the basic assumption that the constitutive relations are defined on a fault plane without thickness.   As Barka and Kadinsky-Cade [1988] reported for earthquakes in Turkey, the ruptures of earthquake do not propagate past stepovers that are wider than 5 km, which roughly limits the wavelength that can regard a fault zone as a plane without thickness in the analysis of large earthquakes.   The resolution of my analysis is of this order, and more detailed analysis must overcome this limitation.   The method of this study may be impossible with the exception of smaller earthquakes and rare large earthquakes whose fault system can be successfully represented by a plane.

Nevertheless, it is still important to estimate constitutive relations even with poor resolution, as long as the difference of the relations can be detected as in this study.   As example, small slip-weakening rates may exist in many earthquakes in the shallow region of the fault plane, since earthquake damage is sometimes anomalously low along the surface ruptured fault trace when large earthquake occurs, which cannot be explained if shallow slip obeys a classical friction law of static and dynamic friction.   This implies that the constitutive relations in the shallow crust have great significance to strong-motion displacement excited near fault planes in practical use.   As another example, small slip-weakening rate may be a candidate to explain slipping behavior of so-called slow earthquakes having long rise time, expected from the negative correlation between rise time and slip-weakening rate.   If analysis with high resolution is possible, more discussion is possible about constitutive relation in many aspects of the earthquake source.   By accumulation of study about constitutive relations of actual earthquakes, the complexity and diversity of the earthquake source will be understood with the various constitutive relations and the physics behind them.

Acknowledgments

References

Akaike, H, Likelihood and Bayes procedure, in *Bayesian Statistics*, edited by J. M. Bernardo, M. H. DeGroot, D. V. Lindley, and A. F. M. Smith, pp. 143-166, University Press, Valencia, Spain, 1980.

Aki, K. and P. G. Richards, *Quantitative Seismology: Theory and Methods*, W. H. Freeman, New York, 1980.

Alterman Z. and F. C. Karal, Propagation of elastic waves in layered media by finite difference methods, *Bull. Seismol. Soc. Am.*, *58*, 367-398, 1968.

Andrews, D. J., Rupture propagation with finite stress in antiplane strain, *J. Geophys. Res.*, *81*, 3575-3582, 1976.

Andrews, D. J., Dynamic plane-strain shear rupture with a slip-weakening friction law calculated by a boundary integral method, *Bull. Seismol. Soc. Am.*, *75*, 1-21, 1985.

Aoki, H. and I. Muramatsu, Crustal structure in the profile across Kinki and Shikoku, Japan, as derived from Miboro and the Toyama explosions, *Zishin 2*, *27*, 104-109, 1973.

Archuleta, R. J., A faulting model for the 1979 Imperial Valley earthquake, *J. Geophys. Res.*, *89*, 4559-4585, 1984.

Awata, Y., K. Mizuno, Y. Sugiyama, K. Shimokawa, R. Imura, and K. Kimura, Surface faults associated with the Hyogoken-nanbu earthquake of 1995 (in Japanese), *Chishitsu News*, *486*, 16-20, 1995.

Barenblatt, G. I., The formation of equilibrium cracks during brittle fracture: general ideas and hypotheses, *J. Appl. Math. Mech.*, *23*, 622-636, 1959.

Barka, A. A. and K. Kadinsky-Cade, Strike-slip fault geometry in Turkey and its influence on earthquake activity, *Tectonics, 7*, 663-684, 1988.

Beeler, N. M. and T. E. Tullis, Self-healing slip-pulses in dynamic rupture models due to velocity-dependent strength, *Bull. Seismol. Soc. Am., 86*, 1130-1148, 1996.

Ben-Zion, Y., Stress, slip, and earthquakes in models of complex single-fault systems incorporating brittle and creep deformations, *J. Geophys. Res., 101*, 5677-5706, 1996.

Bouchon, M., A simple method to calculate Green's functions for elastic layered media, *Bull. Seismol. Soc. Am., 71*, 959-971, 1981.

Cao, T. and K. Aki, Effect of slip rate on stress drop, *Pure Appl. Geophys., 124*, 515-529, 1986.

Carlson, J. M. and J. S. Langer, Mechanical model of an earthquake fault, *Phys. Rev. A., 40*, 6470-6484, 1989.

Cochard, A. and R. Madariaga, Dynamic friction under rate-dependent friction, *Pure Appl. Geophys.,* 142, 419-445, 1994.

Cohee, B. P. and G. C. Beroza, Slip distribution of the 1992 Landers earthquake and its implications for earthquake source mechanics, *Bull. Seismol. Soc. Am., 84*, 692-712, 1994.

Cotton, F. and M. Campillo, Frequency domain inversion of strong motions: application to the 1992 Landers earthquake, *J. Geophys. Res., 100*, 3961-3975, 1995.

Day, S. M., Three-dimensional finite difference simulation of fault dynamics: rectangular faults with fixed rupture velocity, *Bull. Seismol. Soc. Am., 72*, 705-727, 1982.

Dieterich, J. H., Modeling of rock friction: 1. Experimental results and constitutive equations, *J. Geophys. Res., 84*, 2161-2168, 1979.

Dieterich, J. H., Earthquake nucleation on faults with rate- and state-dependent strength, *Tectonophysics, 211*, 115-134, 1992.

Ellsworth, W. L., Nucleation of the Hyogo-ken Nanbu (Kobe), Japan earthquake, *Eos Trans. AGU*, *76*, F372, 1995.

Fukuyama, E., and T. Mikumo, Dynamic rupture analysis: inversion for the source process of the 1990 Izu-Oshima, Japan, Earthquake (M = 6.5), *J. Geophys. Res., 98*, 6529-6542, 1993.

Hartzell, S. H. and T. H. Heaton, Inversion of strong ground motion and teleseismic waveform data for the fault rupture history of the 1979 Imperial Valley, California, earthquake, *Bull. Seismol. Soc. Am., 73*, 1553-1583, 1983.

Hartzell, S. H. and T. H. Heaton, Rupture history of the 1984 Morgan Hill, California, earthquake from the inversion of strong motion records, *Bull. Seismol. Soc. Am., 76*, 649-674, 1986.

Heaton, T. H., Evidence for and implications of self-healing pulses of slip in earthquake rupture, *Phys. Earth Planet. Inter., 64*, 1-29, 1990.

Hirata, N., S, Ohmi, S. Sakai, K. Katsumata, S. Matsumoto, T. Takanami, A. Yamamoto, T. Nishimura, T. Iidaka, T. Urabe, M. Sekine, T. Ooida, F. Yamazaki, H. Katao, Y. Umeda, K. Ito, M. Nakamura, N. Seto, T Matsushima, H. Shimizu, and Japanese University Group of the Urgent Joint Observation for the 1995 Hyogo-ken Nanbu Eaarthquake, Urgent joint observation of aftershocks of the 1995 Hyogo-ken nanbu earthquake, *J. Phys. Earth*, in press, 1996.

Horikawa, H. , K. Hirahara, Y. Umeda, M. Hashimoto, and F. Kusano, Simultaneous inversion of geodetic and strong motion data for the source process of the Hyogo-ken Nanbu, Japan, earthquake, *J. Phys. Earth*, in press, 1996.

Ida, Y., Cohesive force across the tip of a longitudinal-shear crack and Griffith's specific surface energy, *J. Geophys. Res., 77*, 3796-3805, 1972.

Ide, S., F. Imamura, Y. Yoshida, and K. Abe, Source characteristics of the Nicaraguan tsunami earthquake of September 2, 1992, *Geophys. Res. Lett., 20*, 863-866, 1993.

73

Ide, S. and M. Takeo, The dynamic rupture process of the 1993 Kushiro-oki earthquake, *J. Geophys. Res., 101*, 5661-5675, 1996.

Ide, S., M. Takeo, and Y. Yoshida, Source process of the 1995 Kobe earthquake: determination of spatio-temporal slip distribution by Bayesian modeling, *Bull. Seismol. Soc. Am., 86*, 547-566, 1996a.

Ide, S., M. Takeo, and Y. Yoshida, Source model of the 1995 Hyogo-ken Nanbu earthquake determined by near-field strong motion records, *J. Phys. Earth*, in press, 1996b.

Jackson, D. D. and M. Matsu'ura, A Bayesian approach to nonlinear inversion, *J. Geophys. Res., 90*, 581-591, 1985.

Kanamori, H., Mechanics of tsunami earthquakes, *Phys. Earth Planet. Inter., 6*, 346-359, 1972.

Katsumata, A., Comparison between JMA-87 and mechanical seismometers (in Japanese), *Programme Abstr. Jpn. Seismol. Soc., 2*, 245, 1989.

Kawakatsu, H., Automated near-realtime CMT inversion, *Geophys. Res. Lett., 22*, 2569-2572, 1995.

Kennet, B. L. N and N. J. Kerry, Seismic waves in a stratified half space, Geophys. *J. R. Astron. Soc., 57*, 557-583, 1979.

Kikuchi, M. and H. Kanamori, Inversion of complex body waves - III, *Bull. Seismol. Soc. Am., 81*, 2335-2350, 1991.

Lawson, C. L. and R. J. Hanson, *Solving Least Squares Problems*, Prentice-Hall, Inc., Englewood Cliffs., New Jersey, 1984.

Madariaga, R., Dynamics of an expanding circular fault, *Bull. Seismol. Soc. Am., 66*, 639-666, 1976.

Marone, C. and B. Kilgore, Scaling of the critical slip distance for seismic faulting with shear strain in fault zones, *Nature, 362*, 618-621, 1993.

Marone, C, C. B. Raleigh, and C. H. Scholz, Frictional behavior and constitutive modeling of simulated fault gouge, *J. Geophys. Res., 95*, 7007-7025, 1990.

Marone, C. and C. H. Scholz, The depth of seismic faulting and the upper transition from stable to unstable slip regimes, *Geophys. Res. Lett., 15*, 621-624, 1988.

Marone, C. , C. H. Scholz, and R. Bilham, On the mechanics of earthquake afterslip, *J. Geophys. Res., 96*, 8441-8452, 1991.

Matsu'ura, M., H. Kataoka, and B. Shibazaki, Slip-dependent friction law and nucleation processes in earthquake rupture, *Tectonophysics, 211*, 135-148, 1992.

Mikumo, T., K. Hirahara, and T. Miyatake, Dynamical fault rupture process in heterogeneous media, *Tectonophysics, 144*, 19-36, 1987.

Miyatake, T., Reconstruction of dynamic rupture process of an earthquake with constraints of kinematic parameters, *Geophys. Res. Lett., 19*, 349-352, 1992.

Nakamura, M. and M. Ando, Aftershock distribution of the January 17, 1995 Kobe earthquake determined by the JHD method, *J. Phys. Earth*, in press, 1996.

Nakata, T. and K., Yomogida, Surface fault characteristics of the 1995 Hyogoken-nambu earthquake, *J. Natural Disast. Sci., 16*, 1-9, 1995.

Ohnaka, M, Y. Kuwahara, and K. Yamamoto, Constitutive relations between dynamic physical parameters near a tip of the propagating slip zone during stick-slip shear failure, *Tectonophysics, 144*, 109-125, 1987.

Okubo, P. G., Dynamic rupture modeling with laboratory-derived constitutive relations, *J. Geophys. Res., 94*, 12321-12335, 1989.

Okubo, P. G. and J. H. Dieterich, Effects of physical fault properties on frictional instabilities produced on simulated faults, *J. Geophys. Res., 89*, 5817-5827, 1984.

Olson, A. H. and R. J. Aspel, Finite faults and inverse theory with applications to the 1979 Imperial Valley earthquake, *Bull. Seismol. Soc. Am., 72*, 1969-2001, 1982.

Papageorgiou, A. S. and K. Aki, A specific barrier model for the quantitative description of inhomogeneous faulting and the prediction of strong ground motion: II. applications of the model, *Bull. Seismol. Soc. Am., 73*, 953-978, 1983.

Quin, H., Dynamic stress drop and rupture dynamics of the October 15, 1979 Imperial Valley, California, earthquake, *Tectonophysics, 175*, 93-117, 1990.

Research Group for Active Faults of Japan, *Active faults in Japan: sheet maps and inventories*, University of Tokyo Press, 1991.

Rice, J., Spatio-temporal complexity of slip on a fault, *J. Geophys. Res., 98*, 9885-9907, 1993.

Ruina, A., Slip instability and state variable friction law, *J. Geophys. Res., 88*, 10359-10370, 1983.

Scholz, C. H., The critical slip distance for seismic faulting, *Nature, 336*, 761-763, 1988.

Scholz, C. H., *The Mechanics of Earthquakes and Faulting*, Cambridge University Press, New York, 1990.

Sekiguchi H., K. Irikura, T. Iwata, Y. Kakehi, and M. Hoshiba, Minute locating of fault planes and source process of the 1995 Hyogo-ken Nanbu (Kobe), Japan, earthquake from the waveform inversion of strong ground motion, *J. Phys. Earth*, in press, 1996.

Shibazaki, B. and M. Matsu'ura, Spontaneous process for nucleation, dynamic propagation, and stop of earthquake rupture, *Geophys. Res. Lett., 19*, 1189-1192, 1992.

Shibazaki, B. and M. Matsu'ura, Foreshocks and pre-events associated with the nucleation of large earthquakes, *Geophys. Res. Lett., 22*, 1305-1308, 1995.

Takeo, M., S. Ide, and Y. Yoshida, The 1993 Kushiro-oki earthquake: a high stress-drop event in a subducting slab, *Geophys. Res. Lett., 20*, 2607-2610, 1993.

Takeo, M, Near-field synthetic seismograms taking into account the effects of anelasticity: the effects of anelastic attenuation on seismograms caused by a sedimentary layer (in Japanese), *Meteorol. Geophys., 36*, 245-257, 1985.

Takeo, M, The rupture process of the 1989 Offshore Ito earthquakes preceding a submarine volcanic eruption, *J. Geophys. Res., 97*, 6613-6627, 1992.

Tse, S. T. and J. R. Rice, Crustal earthquake instability in relation to the depth variation of frictional slip properties, *J. Geophys. Res., 91*, 9452-9472, 1986.

Utsu, T., *Seismology Second Edition* (in Japanese), Kyoritsu Shuppan, Tokyo, Japan, 1984.

Wald, D. J., Slip history of the 1995 Kobe, Japan, earthquake determined from strong motion, teleseismic, and geodetic data, *J. Phys. Earth*, in press, 1996.

Wald, D. J. and T. H. Heaton, Spatial and temporal distribution of slip for the 1992 Landers, California, earthquake, *Bull. Seismol. Soc. Am., 84*, 668-691, 1994.

Wald, D. J., T. H. Heaton, and K. W. Hudnut, The slip history of the 1994 Northridge, California, earthquake determined from strong-motion, teleseismic, GPS, and leveling data, *Bull. Seismol. Soc. Am., 86*, 49-70, 1996.

Wald, D. J., D. V. Helmberger, and T. H. Heaton, Rupture model of the 1989 Loma Prieta earthquake from the inversion of strong-motion and broadband teleseismic data, *Bull. Seismol. Soc. Am., 81*, 1540-1572, 1991.

Yabuki, T. and M. Matsu'ura, Geodetic data inversion using a Bayesian information criterion for spatial distribution of fault slip, *Geophys. J. Int., 109*, 363-375, 1992.

Yoshida, S., Waveform inversion using ABIC for the rupture process of the 1983 Hindu Kush earthquake, *Phys. Earth Planet. Inter., 56*, 389-405, 1989.

Yoshida, S., Waveform inversion for rupture process using a non-flat seafloor model: application to 1986 Andreanof Island and 1985 Chile earthquake, *Tectonophysics, 211*, 45-59, 1992.

Yoshida, S. and K. Koketsu, Simultaneous inversion of waveform and geodetic data for the rupture process of the 1984 Naganoken-Seibu, Japan, earthquake, *Geophys. J. Int., 103*, 355-362, 1990.

Yoshida, S., K. Koketsu, B. Shibazaki, T. Sagiya, T. Kato, and Y Yoshida, Joint inversion of near- and far-field waveforms and geodetic data for the rupture process of the 1995 Kobe earthquake, *J. Phys. Earth*, in press, 1996.

Yoshida, Y. and T. Yokota, Magnitude determined from *P*-wave amplitude (in Japanese), *Programme Abstr. Jpn. Seismol. Soc., 2*, 11 ,1994.